ESAIM: M2AN 57 (2023) 2371–2396
https://doi.org/10.1051/m2an/2023051

ESAIM: Mathematical Modelling and Numerical Analysis
www.esaim-m2an.org

DISCRETE-TIME ANALYSIS OF OPTIMIZED SCHWARZ WAVEFORM RELAXATION WITH ROBIN PARAMETERS DEPENDING ON THE TARGETED ITERATION COUNT

Arthur Arnoult[1], Caroline Japhet[1] and Pascal Omnes[1,2,*]

Abstract. We propose a new approach that provides new results in the convergence analysis of optimized Schwarz waveform relaxation (OSWR) iterations for parabolic problems, and allows to define efficient optimized Robin parameters that depend on the targeted iteration count, a property that is shared by the actual observed optimal parameters, while traditional Fourier analysis in the time direction leads to iteration independent parameters. This new approach is based on the exact resolution of the time semi-discrete error equations. It allows to recommend a couple (number of iterations, Robin parameter) to reach a given accuracy. While the general ideas may apply to an arbitrary space dimension, the analysis is first presented in the one dimensional case. Numerical experiments illustrate the performance obtained with such iteration-dependent optimized Robin parameters.

Mathematics Subject Classification. 65M55, 35K20, 65M12, 65M22, 65B99.

Received August 26, 2022. Accepted June 2, 2023.

1. Introduction

Schwarz waveform relaxation (SWR) algorithms [12, 17, 22], and their extensions, have a long history in the parallel solution of discretized time-dependent models driven by partial differential equations, such as those arising in engineering, physics, porous media or geophysical applications, etc [1, 4, 6, 8, 10, 20, 25, 29, 36, 39, 41]. The success of these iterative methods is linked to their fast convergence that can be optimized by choosing appropriate boundary conditions on the space-time interfaces between subdomains. In this contribution, we consider Robin boundary conditions without overlap, in which the value of the Robin parameter(s) can be chosen identically on the two sides of the interface (the so-called one-sided case), or differently (the two-sided case), and can be optimized to improve convergence rates. The corresponding algorithm is called optimized Schwarz waveform relaxation (OSWR), see [15, 20, 35]. These methods are well-suited to handle nonconformities in time and space, and can be combined with *a posteriori* estimates (to get efficient stopping criteria) or time parallelization techniques [2, 7, 21, 24, 26].

Keywords and phrases. Optimized Schwarz waveform relaxation discrete-time convergence analysis, iteration-dependent Robin parameters.

[1] Université Sorbonne Paris Nord, LAGA, CNRS UMR 7539, Institut Galilée, 99 Av. J.-B. Clément, 93430 Villetaneuse, France.
[2] Université Paris-Saclay, CEA, Service de Génie Logiciel pour la Simulation, 91191 Gif-sur-Yvette, France.
*Corresponding author: pascal.omnes@cea.fr

© The authors. Published by EDP Sciences, SMAI 2023

This is an Open Access article distributed under the terms of the Creative Commons Attribution License (https://creativecommons.org/licenses/by/4.0), which permits unrestricted use, distribution, and reproduction in any medium, provided the original work is properly cited.

Traditional convergence analysis of OSWR algorithms is mostly performed using the continuous model, in an attempt to obtain a theory which is independent of the actual numerical schemes used for discretization. This analysis may be performed by energy estimates, both in the one-sided and two-sided cases [26, 28]. This technique is quite general but does not provide a convergence rate, nor a hint on how to properly choose the Robin parameters for fast convergence. At the discrete-time level, a convergence proof by energy estimates is performed for the one-sided case [26], but not for the two-sided case.

On the other hand, Fourier transforms in time and space are commonly used at the continuous level to obtain convergence rates of the OSWR method for each Fourier mode [3, 13, 15, 20, 30, 35]; although the supremum of this convergence factor over the whole Fourier space is one, it can however be used to choose efficient Robin parameters that optimize it over the bounded range of frequencies relevant to the discrete numerical (time and space) grids. However, actual numerical results obtained with this choice of Robin parameters do not always perform as efficiently as expected and it has been discussed that this problem may be linked to the Fourier transform in time that may not always allow to perform an adequate analysis of the convergence properties of the method [16, 38]. This may be due to the fact that the Fourier transform supposes an infinite time interval, while the actual simulation is necessarily performed on a finite one; switching to Fourier series does not solve this issue since the error does not vanish at the final time as it does at the initial time. Another approach, based on discrete-time analysis is proposed in [9, 27]; for simple schemes, it is based on the so-called one-sided $\mathcal{Z}$ transform, which is a discrete equivalent of the Laplace transform. However, this also requires either to consider infinite intervals in time or to neglect the error at the final time. On the contrary, in the present contribution we do not perform any transformation in the time direction; restricting for the sake of simplicity to the one-dimensional heat equation, we solve directly the full space-time semi-discrete system on any finite time interval; this is made possible by the Jordan form of the backward Euler scheme that is used to discretize in the time direction. The extension to higher dimensions with domain decompositions that contain cross-points is more complex and is the subject of a separate work.

This approach is particularly rich and allows to obtain several new results: first, we prove convergence of the discrete-time one-sided and two-sided algorithms for any positive value of the Robin coefficients, with a convergence that, for any fixed value of the number of time steps, depends on a single parameter in the one-sided case (and on two parameters in the two-sided case) which is a combination of the diffusion coefficient value, the time step and the Robin parameter; secondly, we obtain exact convergence of the OSWR for a well-chosen value of the Robin parameters in a number of iterations equal to the number of time steps (one-sided case) or twice this number (two-sided case). Furthermore, numerical simulations show that the observed optimal Robin parameter depends itself on the number of iterations performed, and we propose a method to choose an efficient parameter as a function of this number; this allows us to recommend a couple (number of iterations, Robin parameter) to reach a given accuracy, *e.g.* the expected scheme accuracy.

This paper is organized as follows: in Section 2, we consider a model problem and state its well-posedness, as well as that of the equivalent multi-domain problem. Then we introduce the discrete-time multi-domain problem, using an implicit Euler scheme. This problem involves a matrix on which our analysis depends; some of its properties are given in Section 3. In Section 4, we first recall the continuous OSWR method, and the usual approach to calculate optimized Robin parameters using Fourier transform in time. Then we consider the discrete-time OSWR algorithm and prove its convergence, as well as various related properties. The main result of this article is an estimate of the relative convergence error at each iteration, which allows to introduce a new strategy to define discrete-time optimized parameters that depend on the number of iterations that will be performed. Finally, in Section 5, numerical experiments show that the proposed error estimate is close to the relative convergence error at each iteration. Numerical results comparing convergence with continuous or discrete-time optimized Robin parameters show that, even if the continuous ones can be a reasonable choice in some cases, the discrete-time ones give better performances, as they are close to the iteration dependent numerical optimal ones, in all test cases. Asymptotic performance with these optimized parameters shows that the convergence depends weakly (one-sided) and is almost independent (two-sided) of the time step.

2. Problem setting

In order to simplify the analysis, we consider the following monodimensional heat equation on $\Omega \times (0,T)$, with $\Omega = \mathbb{R}$ and $T > 0$ the final time,

$$\begin{aligned} &\mathcal{L}u \coloneqq \partial_t u - \nu \partial_{xx} u = f && \text{in } \Omega \times (0,T), \\ &u(\cdot\,, t=0) = u_0 && \text{in } \Omega, \\ &\lim_{x \to \pm\infty} u(x,\cdot) && \text{is bounded on } (0,T), \end{aligned} \tag{1}$$

where f is a source term, u_0 an initial condition and ν a positive diffusion coefficient.

Let $H^{r,s}(\Omega \times (0,T)) = L^2(0,T;H^r(\Omega)) \cap H^s(0,T;L^2(\Omega))$ be anisotropic Sobolev spaces defined in [33]. Let us recall Propositions 2.1 and 2.2 below, that can be directly deduced from [34].

Proposition 2.1. *If u_0 belongs to $H^1(\Omega)$ and f to $L^2(0,T;L^2(\Omega))$, then problem (1) admits a unique solution in $H^{2,1}(\Omega \times (0,T))$.*

Let us consider a decomposition of Ω into two non-overlapping subdomains

$$\Omega_1 = (-\infty, 0), \quad \Omega_2 = (0, +\infty),$$

and introduce the Robin interface operators as follows (see [15,32])

$$\mathcal{B}_1 = \nu \partial_x + \alpha_1, \qquad \mathcal{B}_2 = -\nu \partial_x + \alpha_2. \tag{2}$$

Then, problem (1) can be reformulated as the following equivalent multi-domain problem, with $f_i = f_{|\Omega_i}$, $u_i = u_{|\Omega_i}$, and $u_{0,i} = u_{0|\Omega_i}$, $i = 1,2$:

$$\begin{aligned} &\mathcal{L}u_1 = f_1 && \text{in } \Omega_1 \times (0,T), && \mathcal{L}u_2 = f_2 && \text{in } \Omega_2 \times (0,T), \\ &\mathcal{B}_1 u_1 = \mathcal{B}_1 u_2 && \text{on } \{0\} \times (0,T), && \mathcal{B}_2 u_2 = \mathcal{B}_2 u_1 && \text{on } \{0\} \times (0,T), \\ &u_1(\cdot,0) = u_{0,1} && \text{in } \Omega_1, && u_2(\cdot,0) = u_{0,2} && \text{in } \Omega_2, \\ &\lim_{x \to -\infty} u_1(x,\cdot) && \text{is bounded on } (0,T), && \lim_{x \to +\infty} u_2(x,\cdot) && \text{is bounded on } (0,T). \end{aligned} \tag{3}$$

The Robin parameters α_1, α_2 involved in (3) (through $\mathcal{B}_i$, $i = 1,2$, defined in (2)) are freely chosen positive real numbers taken such that: (a) the Robin subdomain problems in (3) are well posed (see *e.g.* [7,34]), (b) they lead to a fast converging OSWR algorithm (see Sect. 4).

Proposition 2.2. *Let $i = 1$ or $i = 2$. If $u_{0,i} \in H^1(\Omega_i)$, $f_i \in L^2(0,T;L^2(\Omega_i))$, and $\mathcal{B}_i u_j \in H^{\frac{1}{4}}(0,T)$, with $j = 3 - i$, then the Robin subdomain problem in Ω_i in (3) has a unique solution in $H^{2,1}(\Omega_i \times (0,T))$.*

In practice, a problem such as (3) is solved approximately through discretization and approximation of the derivatives of u by discrete formulas. In this article, we are concerned with the implicit Euler approximation of the time derivative, with uniform time step $\Delta t = \frac{T}{N}$ ($N \in \mathbb{N}^*$). Thus, we consider the following semi-discrete approximation of (3): Find $U_i = (U_{i,1} \dots U_{i,N})^T$, for $i = 1,2$, such that

$$\begin{aligned} &LU_1 = F_1 && \text{in } \Omega_1, && LU_2 = F_2 && \text{in } \Omega_2, \\ &B_1 U_1 = B_1 U_2 && \text{at } x = 0, && B_2 U_2 = B_2 U_1 && \text{at } x = 0, \\ &\lim_{x \to -\infty} U_1(x) && \text{is bounded}, && \lim_{x \to +\infty} U_2(x) && \text{is bounded}, \end{aligned} \tag{4}$$

with operator $L : (H^2(\Omega_i))^N \to (L^2(\Omega_i))^N$, $i = 1,2$, defined as follows

$$LU_i \coloneqq \frac{1}{\nu \Delta t} A U_i - U_i'',$$

where $A \in \mathbb{R}^{N\times N}$ is defined by

$$A \coloneqq \begin{pmatrix} 1 & & & \\ -1 & 1 & & \\ & \ddots & \ddots & \\ & & -1 & 1 \end{pmatrix}, \tag{5}$$

and where, for $i = 1, 2$, for all $n \in [\![1, N]\!]$, for all $x \in \Omega_i$, $U_{i,n}(x)$ is an approximation of $u_i(x, n\Delta t)$, and $F_i = (F_{i,1} \dots F_{i,N})^T$, with $F_{i,n}(x) \coloneqq \frac{f_i(x,n\Delta t)}{\nu} + \frac{u_0(x)}{\nu\Delta t}\delta_{1n}$ (where δ_{1n} is the Kronecker delta). The discrete interface operators B_1 and B_2 are extensions of $\mathcal{B}_1$ and $\mathcal{B}_2$ to vectors in $(H^2(\Omega_i))^N$, *i.e.* for $i = 1, 2$,

$$B_i : U \in \left(H^2(\Omega_i)\right)^N \mapsto (-1)^{i+1}\nu\partial_x U + \alpha_i U. \tag{6}$$

The analysis performed in this article relies on various properties of matrix A, which are presented in the next section.

3. Jordan decomposition

As we will see in Theorem 4.1, solving (4) will involve a square root of matrix A. Therefore, we will prove that it exists, using the Jordan decomposition of A. This decomposition will also be very useful for the analysis of the OSWR algorithm in Section 4.

3.1. Definitions and general results

We recall here some definitions and results about matrix exponential, square root of a matrix and Jordan decomposition, from [23, 37, 40].

Definition 3.1 (Square root of a matrix)**.** A square root of a matrix M is a matrix whose square is M. It might not exist nor be unique.

Definition 3.2 (Matrix exponential)**.** If M is a square matrix, the *exponential of* M is the matrix defined by

$$\exp(M) \coloneqq \sum_{k=0}^{+\infty} \frac{M^k}{k!}.$$

We recall the following property about matrix exponential from [37], Page 79.

Proposition 3.3. *The function $\varphi : x \in \mathbb{C} \mapsto \exp(xM)$, where M is a square matrix, is differentiable with respect to x and $\frac{\partial\varphi}{\partial x}(x) = M\exp(xM) = \exp(xM)M$.*

We recall the following results (Def. 3.4 and Thm. 3.5) about Jordan decomposition from [40], Page 350 and [23], Page 317.

Definition 3.4 (Jordan block)**.** The Jordan block of parameter μ and size r_k is the $r_k \times r_k$ matrix ($r_k \in \mathbb{N}^*$), defined by

$$J_\mu \coloneqq \begin{pmatrix} \mu & 1 & & 0 \\ & \ddots & \ddots & \\ & & \ddots & 1 \\ 0 & & & \mu \end{pmatrix}.$$

Theorem 3.5 (Jordan decomposition)**.** *If $M \in \mathbb{C}^{N\times N}$, then there exists a nonsingular matrix $X \in \mathbb{C}^{N\times N}$ such that*

$$XMX^{-1} = \begin{pmatrix} J_{\mu_1} & & 0 \\ & \ddots & \\ 0 & & J_{\mu_K} \end{pmatrix},$$

where $\mu_1, \dots \mu_K$ are the eigenvalues of M, possibly equal. The number of Jordan blocks associated with an eigenvalue is equal to its geometric multiplicity, i.e. the dimension of the associated eigenspace.

Proposition 3.6 (Commuting two Jordan blocks of same size)**.** *Blocks J_λ and J_μ commute (and thus also J_λ^{-1} and J_μ^{-1}), as well as J_λ^{-1} and J_μ.*

3.2. Square root of a matrix

In this part, we prove that a Jordan matrix admits a square root.

Proposition 3.7. *Every matrix $M = \mu \boldsymbol{I}_N + \mathcal{N}$ with μ nonzero and $\mathcal{N}$ a nilpotent matrix admits a square root under the form*

$$\sqrt{M} \coloneqq \sqrt{\mu} \sum_{k=0}^{N} \binom{\frac{1}{2}}{k} \frac{1}{\mu^k} \mathcal{N}^k, \tag{7}$$

with generalized binomial coefficients:

$$\binom{\frac{1}{2}}{0} \coloneqq 1, \qquad \binom{\frac{1}{2}}{k} \coloneqq \frac{\frac{1}{2}\left(\frac{1}{2}-1\right)\dots\left(\frac{1}{2}-k+1\right)}{k!}, \quad \forall k \geq 1.$$

Proof. Let us start with the case where $\mu = 1$. Let d be the index of $\mathcal{N}$. If $d = 1$, then $\mathcal{N} = 0_{N,N}$, thus $M = \mathbf{I}_N$, and (7) gives $\sqrt{M} = \mathbf{I}_N$, which is indeed a square root of M. If $d > 1$, let

$$P_{d-1}(X) \coloneqq \sum_{k=0}^{d-1} \binom{\frac{1}{2}}{k} X^k.$$

We will prove that $P_{d-1}^2(\mathcal{N}) = \mathbf{I}_N + \mathcal{N}$, *i.e.* that the polynomial R defined by $R(X) \coloneqq 1 + X - P_{d-1}^2(X)$ vanishes in matrix $\mathcal{N}$. For this, we will first show that R is factorizable as a product of X^d and a polynomial, and then use that $\mathcal{N}^d = 0$.

The polynomial P_{d-1} has been chosen as the $(d-1)$-order Taylor expansion of $t \mapsto \sqrt{1+t}$ around 0:

$$\sqrt{1+t} \underset{t\to 0}{=} P_{d-1}(t) + o(t^{d-1}).$$

By squaring the above equality, we get

$$1 + t = \sqrt{1+t}^2 \underset{t\to 0}{=} P_{d-1}^2(t) + 2P_{d-1}(t)o\big(t^{d-1}\big) + o\big(t^{d-1}\big)^2 = P_{d-1}^2(t) + o\big(t^{d-1}\big). \tag{8}$$

The polynomial R being of degree $2d-2$, it can be written under the form $R(X) = \sum_{k=0}^{2d-2} \eta_k X^k$, with $\eta_k \in \mathbb{R}$ and $\eta_{2d-2} \neq 0$. Then, from (8) and the definition of R, one gets $R(t) \underset{t\to 0}{=} o(t^{d-1})$ which is only possible if all η_k are zeros for $k \in [\![0, d-1]\!]$. This implies that

$$R(X) = \sum_{k=d}^{2d-2} \eta_k X^k = \sum_{k=0}^{d-2} \eta_{k+d} X^{k+d} = X^d \sum_{k=0}^{d-2} \eta_{k+d} X^k.$$

Using that $\mathcal{N}$ is a nilpotent matrix of index d, *i.e.* $\mathcal{N}^d = 0$, it follows that $R(\mathcal{N}) = 0$. According to the definition of R, we obtain:

$$\mathbf{I}_N + \mathcal{N} = P_{d-1}^2(\mathcal{N}).$$

Let us now consider the general case, with μ nonzero, arbitrary. We can rewrite M as $M = \mu(\mathbf{I}_N + \frac{1}{\mu}\mathcal{N})$ where the $\frac{1}{\mu}\mathcal{N}$ is nilpotent of index d, and then apply the above result to define $\sqrt{M}$ by

$$\sqrt{M} \coloneqq \sqrt{\mu}\, P_{d-1}\left(\frac{1}{\mu}\mathcal{N}\right),$$

with $\sqrt{\mu}$ a complex number whose square is μ. □

Corollary 3.8. *If μ is nonzero, J_μ admits a square root. In this case, $\mathcal{N}$ is the matrix with 1 on the superdiagonal, and 0 elsewhere. Then the i-th superdiagonal of $\sqrt{J_\mu}$ only contains coefficient $\mu^{\frac{1}{2}-i}\binom{\frac{1}{2}}{i}$.*

3.3. Application to matrix A

Let us now prove that matrix A (defined in (5)) admits a square root and give the Jordan decomposition of the latter. The following proposition is immediate.

Proposition 3.9 (Eigenvalue and eigenspace of A)**.** *The only eigenvalue of A is 1 and the associated eigenspace is of dimension one:*

$$S_1(A) \coloneqq \mathrm{Span}\big((0,\dots,0,1)^{\mathrm{T}}\big). \tag{9}$$

Proposition 3.10 (Definition and properties of $\sqrt{A}$)**.** *Matrix A admits a square root with the following properties:*

(i) *The only eigenvalue of $\sqrt{A}$ is 1 and the associated eigenspace is $S_1(A)$ defined in (9).*
(ii) *$\sqrt{A}$ admits a Jordan decomposition*

$$\sqrt{A} = Q^{-1}J_1Q, \tag{10}$$

with Q an invertible matrix and J_1 as in Definition 3.4 with $\mu = 1$, $r_k = N$.

Proof. Since $A = \mathbf{I}_N + \mathcal{N}$, where $\mathcal{N}$ is the strictly lower triangular matrix with coefficient -1 on the first lower diagonal, Proposition 3.7 shows that A admits a square root given by formula (7), which additionally shows that 1 is the only eigenvalue of $\sqrt{A}$, since all powers of $\mathcal{N}$ are also strictly lower triangular.

Furthermore, let X be a nonzero eigenvector associated with the eigenvalue of $\sqrt{A}$. We thus have: $\sqrt{A}X = X$. Then $AX = \sqrt{A}\sqrt{A}X = \sqrt{A}X = X$. As X is nonzero, it is also an eigenvector of A, and, according to Proposition 3.9, X is necessarily collinear to $(0,\dots,0,1)^T$. This shows (i).

From (i) and Theorem 3.5, we obtain the Jordan decomposition (ii). □

4. OSWR algorithm

In this section, after recalling some results in the continuous framework, we study the convergence of the discrete-time OSWR algorithm. This will then suggest a methodology for calculating the Robin parameters.

4.1. Continuous case

The OSWR method for solving (3) consists in choosing initial Robin data ξ_1^0, ξ_2^0 on $(0,T)$, and setting $\mathcal{B}_1 u_2^0(0,\cdot) \coloneqq \xi_1^0$, $\mathcal{B}_2 u_1^0(0,\cdot) \coloneqq \xi_2^0$. Then for $\ell = 1, 2, \dots$ one solves the local Robin problems

$$\begin{array}{llll}
\mathcal{L}u_1^\ell = f_1 & \text{in } \Omega_1 \times (0,T), & \mathcal{L}u_2^\ell = f_2 & \text{in } \Omega_2 \times (0,T),\\
\mathcal{B}_1 u_1^\ell = \mathcal{B}_1 u_2^{\ell-1} & \text{on } \{0\} \times (0,T), & \mathcal{B}_2 u_2^\ell = \mathcal{B}_2 u_1^{\ell-1} & \text{on } \{0\} \times (0,T),\\
u_1^\ell(\cdot,0) = u_{0,1} & \text{in } \Omega_1, & u_2^\ell(\cdot,0) = u_{0,2} & \text{in } \Omega_2,\\
\lim\limits_{x\to-\infty} u_1^\ell(x,\cdot) & \text{is bounded,} & \lim\limits_{x\to+\infty} u_2^\ell(x,\cdot) & \text{is bounded.}
\end{array}$$

The usual Fourier transform in time approach (with the assumption of an infinite time interval) provides an expression of the convergence factor of the above algorithm (see [14, 15]) as follows

$$\rho(\omega,\alpha_1,\alpha_2) := \left(\frac{\sqrt{\nu i\omega}-\alpha_1}{\sqrt{\nu i\omega}+\alpha_1}\right)\left(\frac{\sqrt{\nu i\omega}-\alpha_2}{\sqrt{\nu i\omega}+\alpha_2}\right),$$

for all Fourier time frequencies ω. While we have $\max_{\omega\in\mathbb{R}}|\rho(\omega,\alpha_1,\alpha_2)| = 1$, the convergence factor can be used to calculate efficient Robin parameters in the discrete setting. Indeed, in numerical computations the time frequency is bounded, *i.e.* in $[\frac{\pi}{T},\frac{\pi}{\Delta t}]$. Then, one can define *continuous optimized Robin parameters* $\alpha_{1,C}$, $\alpha_{2,C}$ such that

$$|\rho(\omega,\alpha_{1,C},\alpha_{2,C})| = \min_{(\alpha_1,\alpha_2)\in(\mathbb{R}^{+*})^2}\ \max_{\omega\in[\frac{\pi}{T},\frac{\pi}{\Delta t}]}|\rho(\omega,\alpha_1,\alpha_2)|,$$

see *e.g.* [13, 15, 31, 35]. In our numerical experiments of Section 5, the minimization is done using the GNU OCTAVE *fminsearch* function [11].

One can also consider the one-sided case $\alpha := \alpha_1 = \alpha_2$ and define α_C as the solution of the above minimization problem on $\alpha\in\mathbb{R}^{+*}$. Reference [14] gives an explicit formula for α_C when $\nu = 1$. Its extension to any ν through a change of variables provides

$$\alpha_C = \sqrt{\pi\nu}\left(\frac{1}{T\Delta t}\right)^{1/4}.$$

4.2. Dimensionless Robin parameters

In what follows, we will use the notation below, for dimensionless Robin parameters:

$$\bar\alpha_i := \alpha_i\sqrt{\frac{\Delta t}{\nu}},\quad i=1,2,\qquad \bar{\boldsymbol\alpha} := (\bar\alpha_1,\bar\alpha_2). \tag{11}$$

This notation will be useful for the convergence analysis in the discrete-time setting. More precisely, we will observe in Section 4.4 that the convergence depends only on $\bar{\boldsymbol\alpha}$ and N.

Using this notation, the *dimensionless continuous optimized Robin parameters,* for the one and two-sided cases, are respectively denoted by

$$\bar\alpha_C := \sqrt{\pi}\left(\frac{\Delta t}{T}\right)^{1/4},\qquad \bar{\boldsymbol\alpha}_C := \sqrt{\frac{\Delta t}{\nu}}(\alpha_{1,C},\alpha_{2,C}). \tag{12}$$

4.3. Discrete-time algorithm

The discrete-time OSWR algorithm for solving the coupled problem (4) is as follows.

Algorithm 1. Discrete-time OSWR.

Choose initial Robin data $\Xi_1^0,\Xi_2^0\in\mathbb{R}^N$ at $x=0$, and set $B_1U_2^0 := \Xi_1^0$, $B_2U_1^0 := \Xi_2^0$
for $\ell = 1,2,\dots$ **do**
Solve the local Robin problems

$$\begin{array}{llll} LU_1^\ell = F_1 & \text{in } \Omega_1, & LU_2^\ell = F_2 & \text{in } \Omega_2,\\ B_1U_1^\ell = B_1U_2^{\ell-1} & \text{at } x=0, & B_2U_2^\ell = B_2U_1^{\ell-1} & \text{at } x=0,\\ \lim\limits_{x\to-\infty} U_1^\ell(x) & \text{is bounded,} & \lim\limits_{x\to+\infty} U_2^\ell(x) & \text{is bounded.}\end{array} \tag{13}$$

end for

In what follows, an analysis of the convergence of Algorithm 1 is given.

4.4. Discrete-time convergence analysis

Let us denote by (U_1, U_2) the solution of (4). Then, by linearity, the error $E_i^\ell := U_i^\ell - U_i,\ i = 1, 2$, at iteration ℓ of Algorithm 1, satisfies, for $\ell \geq 1$,

$$\begin{aligned} &LE_1^\ell = 0_N && \text{in } \Omega_1, && LE_2^\ell = 0_N && \text{in } \Omega_2, \\ &\lim_{x\to-\infty} E_1^\ell(x) && \text{is bounded}, && \lim_{x\to+\infty} E_2^\ell(x) && \text{is bounded}. \end{aligned} \tag{14}$$

$$B_1E_1^\ell = B_1E_2^{\ell-1} \quad \text{at } x = 0, \qquad B_2E_2^\ell = B_2E_1^{\ell-1} \quad \text{at } x = 0, \tag{15}$$

with

$$B_iE_j^0(0) := \Xi_i^0 - B_iU_i(0), \quad j = 3 - i, \quad i = 1, 2. \tag{16}$$

Then we have the following result:

Theorem 4.1. *Let $\ell \geq 1$. There exists $\beta_i^\ell \in \mathbb{R}^N,\ i = 1, 2$, such that the subdomain solutions of (14) are of the form*

$$E_i^\ell(x) = \mathrm{e}^{\frac{-|x|}{\sqrt{\nu\Delta t}}\sqrt{A}}\beta_i^\ell, \qquad \forall x \in \Omega_i, \quad i = 1, 2. \tag{17}$$

The proof of Theorem 4.1 is given in Appendix A.

Let us introduce the dimensionless initial Robin data for the errors

$$\bar{G}_i^0 := \sqrt{\frac{\Delta t}{\nu}}\big(\Xi_i^0 - (B_iU_i)(0)\big), \quad i = 1, 2. \tag{18}$$

Let us also extend (17) to the case $\ell = 0$, for $\bar{\alpha}_j \neq 1,\ j = 1, 2$,

$$\beta_i^0 := \left(\bar{\alpha}_j\mathbf{I}_N - \sqrt{A}\right)^{-1}\bar{G}_j^0, \qquad j = 3 - i, \quad i = 1, 2, \tag{19}$$

$$E_i^0(x) := \mathrm{e}^{\frac{-|x|}{\sqrt{\nu\Delta t}}\sqrt{A}}\beta_i^0, \qquad \forall x \in \Omega_i, \quad i = 1, 2. \tag{20}$$

For $\ell \geq 1$, the dimensionless Robin data for the errors are denoted by

$$\bar{G}_i^\ell := \sqrt{\frac{\Delta t}{\nu}}\big(B_i\big(E_j^\ell\big)\big)(0) = \left(\bar{\alpha}_i\mathbf{I}_N - \sqrt{A}\right)\beta_j^\ell, \qquad j = 3 - i,\ i = 1, 2. \tag{21}$$

Let $\boldsymbol{H}^1(\Omega_i) := (H^1(\Omega_i))^N$ and $\boldsymbol{L}^\infty(\Omega_i) := (L^\infty(\Omega_i))^N$, equipped respectively with

$$\|U\|_{\boldsymbol{H}^1(\Omega_i)} := \sqrt{\sum_{j\in[\![1,N]\!]}\left(\|U_j\|^2_{H^1(\Omega_i)}\right)}, \quad \|U\|_{\boldsymbol{L}^\infty(\Omega_i)} := \max_{j\in[\![1,N]\!]}\big(\|U_j\|_{L^\infty(\Omega_i)}\big).$$

With these notations and Theorem 4.1, we can now prove the convergence of Algorithm 1.

Theorem 4.2 (OSWR convergence)**.** *Let $\alpha_i > 0$, $i = 1, 2$. Then, Algorithm 1 converges in $(\boldsymbol{H}^1(\Omega_1)\cap\boldsymbol{L}^\infty(\Omega_1))\times(\boldsymbol{H}^1(\Omega_2)\cap\boldsymbol{L}^\infty(\Omega_2))$ to the solution of (4).*

Moreover, setting[1]

$$M(\bar{\boldsymbol{\alpha}}) := \left(\bar{\alpha}_i\boldsymbol{I}_N + \sqrt{A}\right)^{-1}\left(\bar{\alpha}_i\boldsymbol{I}_N - \sqrt{A}\right)\left(\bar{\alpha}_j\boldsymbol{I}_N + \sqrt{A}\right)^{-1}\left(\bar{\alpha}_j\boldsymbol{I}_N - \sqrt{A}\right), \tag{22}$$

we have the following relations on the Robin data for the errors, for $i = 1, 2$,

$$\bar{G}_i^{2\ell} = (M(\bar{\boldsymbol{\alpha}}))^\ell\bar{G}_i^0, \qquad \forall \ell \geq 0, \tag{23a}$$

[1]As all matrices of type $(\bar{\alpha}_i\mathbf{I}_N \pm \sqrt{A})$ and their inverses commute one with the other, matrix M is independent of indices i and j.

$$\bar{G}_i^{2\ell+1} = (M(\bar{\boldsymbol{\alpha}}))^{\ell}\bar{G}_i^1, \qquad \forall \ell \geq 0, \tag{23b}$$

as well as the discrete-time relations for the errors on the interface[2]

$$\beta_i^{2\ell} = (M(\bar{\boldsymbol{\alpha}}))^{\ell}\beta_i^0 \qquad \forall \ell \geq 0, \tag{24a}$$

$$\beta_i^{2\ell+1} = (M(\bar{\boldsymbol{\alpha}}))^{\ell}\beta_i^1 \qquad \forall \ell \geq 0, \tag{24b}$$

from which we deduce the following convergence estimates, for even and odd iterations

$$\frac{\left\|E_i^{2\ell}(0)\right\|_\infty}{\|E_i^0(0)\|_\infty} \leq \left\|(M(\bar{\boldsymbol{\alpha}}))^{\ell}\right\|_\infty, \qquad \forall \ell \geq 0, \tag{25a}$$

$$\frac{\left\|E_i^{2\ell+1}(0)\right\|_\infty}{\|E_i^1(0)\|_\infty} \leq \left\|(M(\bar{\boldsymbol{\alpha}}))^{\ell}\right\|_\infty, \qquad \forall \ell \geq 0. \tag{25b}$$

Thus, $\|(M(\bar{\boldsymbol{\alpha}}))^{\ell}\|_\infty$ is an estimate of the relative L^∞-error at iterations 2ℓ and $2\ell+1$, for all $\ell \geq 0$.

Proof. Let us first prove (23) for $\ell \geq 1$ (the case $\ell = 0$ being trivial).

Using Proposition 3.3, equation (17), and the definition of the Robin operator B_i in (6), we get, for $i = 1, 2$ and $j = 3 - i$:

$$(B_iE_i^{\ell})(0) = \left(\alpha_i\mathbf{I}_N + \nu\frac{\sqrt{A}}{\sqrt{\nu\Delta t}}\right)\beta_i^{\ell}, \quad (B_iE_j^{\ell})(0) = \left(\alpha_i\mathbf{I}_N - \nu\frac{\sqrt{A}}{\sqrt{\nu\Delta t}}\right)\beta_j^{\ell}, \qquad \forall \ell \geq 1.$$

Thus, using (15) and (16) lead to, for $i = 1, 2$,

$$\left(\alpha_i\mathbf{I}_N + \nu\frac{\sqrt{A}}{\sqrt{\nu\Delta t}}\right)\beta_i^1 = \Xi_i^0 - (B_iU_i)(0),$$

$$\left(\alpha_i\mathbf{I}_N + \nu\frac{\sqrt{A}}{\sqrt{\nu\Delta t}}\right)\beta_i^{\ell} = \left(\alpha_i\mathbf{I}_N - \nu\frac{\sqrt{A}}{\sqrt{\nu\Delta t}}\right)\beta_j^{\ell-1}, \quad j = 3 - i, \quad \forall \ell \geq 2,$$

or equivalently, using the dimensionless notations (11) and (18), for $i = 1, 2$,

$$\left(\bar{\alpha}_i\mathbf{I}_N + \sqrt{A}\right)\beta_i^1 = \bar{G}_i^0, \tag{26a}$$

$$\left(\bar{\alpha}_i\mathbf{I}_N + \sqrt{A}\right)\beta_i^{\ell} = \left(\bar{\alpha}_i\mathbf{I}_N - \sqrt{A}\right)\beta_j^{\ell-1}, \quad j = 3 - i, \quad \forall \ell \geq 2. \tag{26b}$$

For $i = 1, 2$, the matrix $(\bar{\alpha}_i\mathbf{I}_N + \sqrt{A})$ is nonsingular. Indeed, using the Jordan decomposition of $\sqrt{A}$ given in (10), and that $\bar{\alpha}_i > 0$, we get

$$\det\left(\bar{\alpha}_i\mathbf{I}_N + \sqrt{A}\right) = \det\left(Q^{-1}(\bar{\alpha}_i\mathbf{I}_N + J_1)Q\right) = \det(\bar{\alpha}_i\mathbf{I}_N + J_1) = (\bar{\alpha}_i + 1)^N \neq 0.$$

Thus, from (26a) and (26b) we obtain, for $i = 1, 2$,

$$\beta_i^2 = \left(\bar{\alpha}_i\mathbf{I}_N + \sqrt{A}\right)^{-1}\left(\bar{\alpha}_i\mathbf{I}_N - \sqrt{A}\right)\left(\bar{\alpha}_j\mathbf{I}_N + \sqrt{A}\right)^{-1}\bar{G}_j^0, \qquad j = 3 - i, \tag{27a}$$

$$\beta_i^{\ell} = M(\bar{\boldsymbol{\alpha}})\beta_i^{\ell-2}, \qquad \forall \ell \geq 3. \tag{27b}$$

[2]Formulas (24a) and (25a) below are only well-defined for $\bar{\alpha}_j \neq 1$, $j = 1, 2$. If $\bar{\alpha}_j = 1$, for $j = 1$ or $j = 2$, we have, for $i = 3 - j$, the equality $\beta_i^{2\ell} = (M(\bar{\boldsymbol{\alpha}}))^{\ell-1}\beta_i^2$ and the convergence estimate $\frac{\|E_i^{2\ell}(0)\|_\infty}{\|E_i^2(0)\|_\infty} \leq \|(M(\bar{\boldsymbol{\alpha}}))^{\ell-1}\|_\infty$, $\forall \ell \geq 1$.

Multiplying now (27a) and (27b) by $(\bar{\alpha}_j \mathbf{I}_N - \sqrt{A})$, with $j = 3-i$, then using that all matrices of type $(\bar{\alpha}_i \mathbf{I}_N \pm \sqrt{A})$ and their inverses commute one with the other, and using (21), we get, for $j = 1, 2$,

$$\bar{G}_j^2 = M(\bar{\boldsymbol{\alpha}})\bar{G}_j^0,$$
$$\bar{G}_j^\ell = M(\bar{\boldsymbol{\alpha}})\bar{G}_j^{\ell-2}, \quad \text{for } \ell \geq 3,$$

from which (23) is deduced by induction. From (27b), we also get (24b) by induction. Then, taking the L^∞-norm of (24b), and using (17), we deduce (25b).

Let us now prove (24a) and (25a). We will distinguish the following cases:

Case $\bar{\alpha}_i \neq 1$, *for* $i = 1, 2$

Multiplying equations (23) by $(\bar{\alpha}_i \mathbf{I}_N - \sqrt{A})^{-1}$ and then using (19) and (21) lead to (24a). Then, taking the L^∞-norm of (24a), and using (17) and (20), we get (25a).

Case $\bar{\alpha}_i = 1$, *for* $i = 1$ *or* $i = 2$

In that case, relations (24a) and (25a) are replaced by $\beta_i^{2\ell} = (M(\bar{\boldsymbol{\alpha}}))^{\ell-1}\beta_i^2$ and $\frac{\|E_i^{2\ell}(0)\|_\infty}{\|E_i^2(0)\|_\infty} \leq \|(M(\bar{\boldsymbol{\alpha}}))^{\ell-1}\|_\infty$, $\forall \ell \geq 1$, respectively (see footnote[2] above). The first relation is obtained by induction from (27b). Then, taking its L^∞-norm, and using (17), we obtain the second one.

Let us now prove that Algorithm 1 converges. Matrix $\sqrt{A}$ is lower triangular with value 1 on the diagonal. Thus, $M(\bar{\boldsymbol{\alpha}})$ is a lower triangular matrix with a unique diagonal coefficient σ, that is its unique eigenvalue, given by

$$\sigma = \left(\frac{\bar{\alpha}_1 - 1}{\bar{\alpha}_1 + 1}\right)\left(\frac{\bar{\alpha}_2 - 1}{\bar{\alpha}_2 + 1}\right).$$

Thus the spectral radius of $M(\bar{\boldsymbol{\alpha}})$ is equal to $|\sigma|$ and strictly smaller than 1, as $\bar{\alpha}_i > 0$.

Consequently, we have $\lim_{\ell\to\infty}(M(\bar{\boldsymbol{\alpha}}))^\ell = 0_{N,N}$, and thus $\lim_{\ell\to\infty}\beta_i^{2\ell} = \lim_{\ell\to\infty}\beta_i^{2\ell+1} = 0_N$, for $i = 1, 2$. Then, from (17) we get $\lim_{\ell\to\infty}\|E_i^{2\ell}\|_{\boldsymbol{L}^\infty(\Omega_i)} = \lim_{\ell\to\infty}\|E_i^{2\ell+1}\|_{\boldsymbol{L}^\infty(\Omega_i)} = 0$, for $i = 1, 2$, as well as $\lim_{\ell\to\infty}\|E_i^{2\ell}\|_{\boldsymbol{H}^1(\Omega_i)} = \lim_{\ell\to\infty}\|E_i^{2\ell+1}\|_{\boldsymbol{H}^1(\Omega_i)} = 0$, $i = 1, 2$, for all positive $\bar{\alpha}_1, \bar{\alpha}_2$, which proves the convergence of Algorithm 1. □

From Theorem 4.2, the following finite convergence results can be derived.

Theorem 4.3 (Finite convergence of OSWR method)**.** *Let* $\bar{\alpha}_i$, $i = 1, 2$, *be the dimensionless Robin parameters defined in* (11).

(i) *If* $\bar{\alpha}_1 = 1$ *or* $\bar{\alpha}_2 = 1$ *(two-sided case), then the OSWR Algorithm 1 converges in at most* $2N + 2$ *iterations;*
(ii) *If* $\bar{\alpha}_1 = \bar{\alpha}_2 = 1$ *(one-sided case), then the OSWR Algorithm 1 converges in at most* $N + 1$ *iterations.*

Proof. Let us prove (i). Using in (23a) the Jordan decomposition of $\sqrt{A}$ (given in (10)), we get, for $\ell \geq 0$, for $i = 1, 2$

$$\bar{G}_i^{2\ell} = Q^{-1}\Big((\bar{\alpha}_i \mathbf{I}_N + J_1)^{-1}(-\bar{\alpha}_i \mathbf{I}_N + J_1)(\bar{\alpha}_j \mathbf{I}_N + J_1)^{-1}(-\bar{\alpha}_j \mathbf{I}_N + J_1)\Big)^\ell Q\,\bar{G}_i^0.$$

Using Property 3.6, the four matrices commute one with the other (as each matrix is a Jordan matrix, *e.g.* $\bar{\alpha}_i \mathbf{I}_N + J_1 = J_{1+\bar{\alpha}_i}$). Then, we have:

$$\bar{G}_i^{2\ell} = Q^{-1}(\bar{\alpha}_i \mathbf{I}_N + J_1)^{-\ell}(-\bar{\alpha}_i \mathbf{I}_N + J_1)^\ell(\bar{\alpha}_j \mathbf{I}_N + J_1)^{-\ell}(-\bar{\alpha}_j \mathbf{I}_N + J_1)^\ell Q\,\bar{G}_i^0. \tag{28}$$

Let $i = 1$ or $i = 2$, and $j = 3 - i$. Let $\bar{\alpha}_i = 1$ (and $\bar{\alpha}_j$ arbitrary). Then the matrix $-\bar{\alpha}_i \mathbf{I}_N + J_1$ has all its coefficients zero, except the superdiagonal ones. Thus, $-\bar{\alpha}_i \mathbf{I}_N + J_1$ is an $N \times N$ nilpotent matrix of index N. Consequently, from (28) with $\ell = N$, we have $\bar{G}_i^{2N} = 0_N$. Using now relations (26b) and (21), we obtain

$$\beta_i^{\ell+1} = \Big(\bar{\alpha}_i \mathbf{I}_N + \sqrt{A}\Big)^{-1}\Big(\bar{\alpha}_i \mathbf{I}_N - \sqrt{A}\Big)\beta_j^\ell = \Big(\bar{\alpha}_j \mathbf{I}_N + \sqrt{A}\Big)^{-1}\bar{G}_i^\ell,$$

and thus we obtain $\beta_i^{2N+1} = 0_N$, and with (26b) we also have

$$\beta_j^{\ell+2} = \left(\bar{\alpha}_j \mathbf{I}_N + \sqrt{A}\right)^{-1}\left(\bar{\alpha}_j \mathbf{I}_N - \sqrt{A}\right)\beta_i^{\ell+1},$$

thus $\beta_j^{2N+2} = 0_N$. Finally, from (17), we get $E_i^{2N+2} = 0_N$, $i = 1, 2$.

Let us now prove (ii). Taking $\bar{\alpha}_1 = \bar{\alpha}_2 = 1$ and multiplying both equations of (26) by $(\mathbf{I}_N - \sqrt{A})$, one gets:

$$\begin{aligned}
\bar{G}_j^1 &= \left(\mathbf{I}_N + \sqrt{A}\right)^{-1}\left(\mathbf{I}_N - \sqrt{A}\right)\bar{G}_i^0,\\
\bar{G}_j^\ell &= \left(\mathbf{I}_N + \sqrt{A}\right)^{-1}\left(\mathbf{I}_N - \sqrt{A}\right)\bar{G}_i^{\ell-1}, \quad j = 3 - i, \quad \forall \ell \geq 2.
\end{aligned}$$

Thus, by induction, we obtain

$$\bar{G}_j^\ell = \left(\mathbf{I}_N + \sqrt{A}\right)^{-\ell}\left(\mathbf{I}_N - \sqrt{A}\right)^{\ell}\bar{G}_{i/j}^0,$$

where $\bar{G}_{i/j}^0$ is $\bar{G}_j^0$ if ℓ is even, $\bar{G}_i^0$ is ℓ is odd.

Using the Jordan decomposition of $\sqrt{A}$ in the above equality (as in (i)), we get

$$\bar{G}_j^\ell = Q^{-1}(\mathbf{I}_N + J_1)^{-\ell}(\mathbf{I}_N - J_1)^{\ell} Q \bar{G}_{i/j}^0.$$

Then, if $\ell = N$, one gets that $\bar{G}_j^N = 0$, $j = 1, 2$, and thus, using (26b) and (21), we get $\beta_j^{N+1} = (\mathbf{I}_N + \sqrt{A})^{-1}(\mathbf{I}_N - \sqrt{A})\beta_i^N = (\mathbf{I}_N + \sqrt{A})^{-1}\bar{G}_j^N = 0_N$, $j = 1, 2$. Finally, from (17), we have $E_j^{N+1} = 0_N$, for $j = 1, 2$. □

From Theorem 4.2, the following result can be obtained.

Theorem 4.4 (Convergence depending only on $\bar{\boldsymbol{\alpha}}$)**.** *For a given $N \geq 1$, the L^∞-norm convergence of Algorithm 1 depends only on $\bar{\boldsymbol{\alpha}}$.*

Proof. This result directly comes from (24) where M depends only on $\bar{\boldsymbol{\alpha}}$ and on N through its dimension. Indeed, the convergence of the sequence $(\beta_i^\ell)_{\ell \in \mathbb{N}}$, $i = 1, 2$, depends only on $\bar{\boldsymbol{\alpha}}$ and N. Then, using (17) and that $\|E_i^\ell\|_{\boldsymbol{L}^\infty(\Omega_i)} = \|\beta_i^\ell\|_\infty$ $i = 1, 2$, the theorem is proven. □

Remark 4.5. For a given $N \geq 1$ (and thus for a given Δt), once the choice of $\bar{\boldsymbol{\alpha}} = (\bar{\alpha}_1, \bar{\alpha}_2)$ has been performed as recommended in Section 4.5 below, one simply has to choose $\alpha_i = \bar{\alpha}_i \sqrt{\frac{\nu}{\Delta t}}$, $i = 1, 2$, to obtain an efficient convergence which will not depend on ν (as follows from Thm. 4.4).

Remark 4.6 (Notation for matrix M)**.** Throughout the sequel of this paper, the matrix defined in (22) will be denoted by $M(\bar{\alpha})$ in the one-sided case $\bar{\boldsymbol{\alpha}} = (\bar{\alpha}, \bar{\alpha})$, and by $M(\bar{\boldsymbol{\alpha}})$ in the two-sided case $\bar{\boldsymbol{\alpha}} = (\bar{\alpha}_1, \bar{\alpha}_2)$.

Remark 4.7. Note that in (25), one could use the upper bound

$$\left\|(M(\bar{\boldsymbol{\alpha}}))^\ell\right\|_\infty \leq \|M(\bar{\boldsymbol{\alpha}})\|_\infty^\ell, \tag{29}$$

and then define Robin parameters, for the one-sided and two-sided cases, respectively denoted by $\bar{\alpha}_M$ and $\bar{\boldsymbol{\alpha}}_M$, as follows

$$\|M(\bar{\alpha}_M)\|_\infty = \min_{\bar{\alpha} \in]0,1]} \|M(\bar{\alpha})\|_\infty, \qquad \|M(\bar{\boldsymbol{\alpha}}_M)\|_\infty = \min_{\bar{\boldsymbol{\alpha}} \in]0,1]^2} \|M(\bar{\boldsymbol{\alpha}})\|_\infty. \tag{30}$$

However, for a given $N \geq 1$, $\|M(\bar{\boldsymbol{\alpha}}_M)\|_\infty^\ell$ is larger than $\|(M(\bar{\boldsymbol{\alpha}}_M))^\ell\|_\infty$, and differs more and more from $\|(M(\bar{\boldsymbol{\alpha}}_M))^\ell\|_\infty$ when ℓ increases. Thus one loses information in the use of the upper bound (29). This will be observed numerically in Section 5.6, where the convergence with $\bar{\boldsymbol{\alpha}}_M$ is much slower (except for the very first iterations) than that with the parameter $\bar{\boldsymbol{\alpha}}$ that minimizes $\|(M(\bar{\boldsymbol{\alpha}}))^\ell\|_\infty$. Consequently, one main objective of this article is to search for discrete-time optimized Robin parameters $\bar{\boldsymbol{\alpha}} = \bar{\boldsymbol{\alpha}}(\ell)$, that depend on iteration ℓ, and minimize $\|(M(\bar{\boldsymbol{\alpha}}))^\ell\|_\infty$. Such parameters will be defined in Section 4.5.

Remark 4.8 (Equivalent writing of discrete-time estimate and notation)**.** From relations (25), the discrete-time estimates at iteration ℓ read

$$\frac{\left\|E_i^\ell(0)\right\|_\infty}{\left\|E_i^0(0)\right\|_\infty} \leq \left\|(M(\bar{\boldsymbol{\alpha}}))^{q(\ell)}\right\|_\infty, \qquad \forall \ell \geq 0 \text{ even}, \tag{31a}$$

$$\frac{\left\|E_i^\ell(0)\right\|_\infty}{\left\|E_i^1(0)\right\|_\infty} \leq \left\|(M(\bar{\boldsymbol{\alpha}}))^{q(\ell)}\right\|_\infty, \qquad \forall \ell \geq 1 \text{ odd}, \tag{31b}$$

$$\text{with} \quad q(\ell) := \begin{cases} \frac{\ell}{2} & \text{if } \ell \text{ is even} \\ \frac{\ell-1}{2} & \text{if } \ell \text{ is odd} \end{cases}, \qquad \forall \ell \geq 0. \tag{32}$$

Thus, $\|(M(\bar{\boldsymbol{\alpha}}))^{q(\ell)}\|_\infty$ is an estimate of the relative L^∞-error at iteration ℓ, for $\ell \geq 0$.

4.5. Choice of the Robin parameters

Let us first consider the one-sided case, *i.e.* $\bar{\alpha} := \bar{\alpha}_1 = \bar{\alpha}_2$. The convergence matrix defined in (22) then reads

$$M(\bar{\alpha}) = \left(\left(\bar{\alpha}\mathbf{I}_N + \sqrt{A}\right)^{-1}\left(\bar{\alpha}\mathbf{I}_N - \sqrt{A}\right)\right)^2, \qquad i = 1, 2.$$

Remarks 4.7 and 4.8 lead us to define a *discrete-time optimized Robin parameter*, denoted by $\bar{\alpha}_{D[\ell]}$, depending on iteration $\ell \geq 2$, as follows (see footnote [3]).

$$\left\|\left(M\left(\bar{\alpha}_{D[\ell]}\right)\right)^{q(\ell)}\right\|_\infty = \min_{\bar{\alpha}\in]0,1]} \left\|(M(\bar{\alpha}))^{q(\ell)}\right\|_\infty, \tag{33}$$

where $q(\ell)$ is defined in (32).

For example, if one wants to optimize the convergence at iteration $\ell = 7$, then one can use the Robin parameter $\bar{\alpha}_{D[7]}$ such that $\|(M(\bar{\alpha}_{D[7]}))^3\|_\infty = \min_{\bar{\alpha}\in]0,1]} \|(M(\bar{\alpha}))^3\|_\infty$.

Remark 4.9. In practice, for the minimization problem in (33), we calculate $\|(M(\gamma_j))^{q(\ell)}\|_\infty$, with $\gamma_j := \frac{j}{100}$ for $j \in [\![1, 100]\!]$, then take the index j_0 that gives the minimum value, and set $\bar{\alpha}_{D[\ell]} = \gamma_{j_0}$.

Note that, although this process requires the repeated inversion of matrices, its cost remains low for the following reasons:

- the matrices are of size N and thus remain of moderate size, since for long time computations a splitting of the time interval into windows is necessary, and one uses the OSWR method in each time window [5, 26];
- the matrices involved at iteration ℓ will be recycled for iteration $\ell+1$, so that the marginal cost of computing the norms of the matrices for an extra iteration remains cheap;
- the calculation of the terms $\|(M(\gamma_j))^{q(\ell)}\|_\infty$, $j \in [\![1, 100]\!]$, can be completely parallelized (with respect to j);
- the method provides a dimensionless optimized parameter $\bar{\alpha}_{D[\ell]}$ whose dependency is only in ℓ and N, and thus independent of the other parameters ν, f, u_0 and of space discretization. It can therefore be calculated only once, at fixed N, whatever the other data of the problem. The (dimensional) optimized Robin parameter is then given by $\alpha_{D[\ell]} := \sqrt{\frac{\nu}{\Delta t}}\bar{\alpha}_{D[\ell]}$.

This process can be extended to the two-sided case with corresponding *two-sided discrete-time optimized parameters* denoted by $\bar{\boldsymbol{\alpha}}_{D[\ell]} = (\bar{\alpha}_{1,D[\ell]}, \bar{\alpha}_{2,D[\ell]})$, as follows :

$$\left\|\left(M\left(\bar{\boldsymbol{\alpha}}_{D[\ell]}\right)\right)^{q(\ell)}\right\|_\infty = \min_{\bar{\boldsymbol{\alpha}}\in]0,1]^2} \left\|(M(\bar{\boldsymbol{\alpha}}))^{q(\ell)}\right\|_\infty, \tag{34}$$

where $M(\bar{\boldsymbol{\alpha}})$ is defined in (22).

[3] The choice of the interval $]0, 1]$ in the minimization problem comes from the fact that the Robin parameters are positive, and from our numerical observations in Section 5.

Remark 4.10. Note that, by definition of $\bar{\alpha}_M$ and $\bar{\boldsymbol{\alpha}}_M$ in (30), and of $\bar{\alpha}_{D[\ell]}$ and $\bar{\boldsymbol{\alpha}}_{D[\ell]}$, $\ell \geq 2$, in (33) and (34) respectively, we have the following relations:

$$\bar{\alpha}_M = \bar{\alpha}_{D[2]} = \bar{\alpha}_{D[3]}, \qquad \bar{\boldsymbol{\alpha}}_M = \bar{\boldsymbol{\alpha}}_{D[2]} = \bar{\boldsymbol{\alpha}}_{D[3]}.$$

5. Numerical results

In this section, some numerical experiments are presented to illustrate the theoretical results of Section 4.

The domain $\Omega = [-\frac{1}{2}, \frac{1}{2}]$ is of length $L_\Omega = 1$. The resolution is done using a finite element code developed in the GNU Octave [11] language, whose mesh size is $\Delta x = 10^{-3}$ (except in Sect. 5.5 where $\Delta x = 5 \times 10^{-5}$). The final time is $T = 1$, and the time step is $\Delta t = \frac{T}{N}$, where N will vary, depending on the numerical examples.

In our test cases we simulate the error equations, *i.e.* we take $u_0 = 0$ and $f = 0$. As the domain is now bounded, we add homogeneous Dirichlet conditions at $x = -\frac{1}{2}$ and $x = \frac{1}{2}$.

We use the OSWR algorithm with the interface at $x = 0$, and with the most general initial Robin data on the interface, under the form of random values, as commonly done in the study of OSWR methods (see *e.g.* [3,19]).

The algorithm is stopped when the L^∞-norm of the jump of the Robin transmission conditions on the interface is smaller than 10^{-12}, unless specified.

In Section 4.4 we have proved that the convergence of the discrete-time OSWR algorithm depends only on dimensionless Robin parameters $\bar{\boldsymbol{\alpha}} = (\bar{\alpha}_1, \bar{\alpha}_2)$ and on N. Thus, in what follows, we will consider only dimensionless Robin parameters $\bar{\alpha}_1, \bar{\alpha}_2$[4].

The solution of the fully discrete error equations at iteration ℓ is denoted $E^\ell_{i,\Delta x}$, and is measured, on the interface[5], either in the L^∞-norm, or in the L^∞-norm scaled by the initial error, as in our theoretical result (31b)[6].

In what follows, we will use the following terms, that are associated to the OSWR iteration ℓ (excepted for the first item in the list below):

- *continuous optimized Robin parameter(s)*: $\bar{\alpha}_C$ or $\bar{\boldsymbol{\alpha}}_C$ given in (12);
- *fully discrete numerical solution*: $E^\ell_{i,\Delta x}$ (as defined above);
- *relative L^∞-error*: error term $\frac{\|E^\ell_{i,\Delta x}(0)\|_\infty}{\|E^1_{i,\Delta x}(0)\|_\infty}$;
- *discrete-time convergence estimate*: upper bound $\|(M(\bar{\boldsymbol{\alpha}}))^{q(\ell)}\|_\infty$ in (31);
- *discrete-time optimized Robin parameter(s)*: $\bar{\alpha}_{D[\ell]}$ or $\bar{\boldsymbol{\alpha}}_{D[\ell]}$, see Section 4.5.

Since the problem is symmetrical for the two domains, the results presented here are only for the left domain (similar results will be obtained for the right domain, up to a permutation of α_1 and α_2 in the two-sided case). Moreover, in the two-sided case, the symmetry implies that the relative error, on odd iterations, obtained with $(\bar{\alpha}_1, \bar{\alpha}_2)$ is the same as with $(\bar{\alpha}_2, \bar{\alpha}_1)$; thus we consider $\bar{\alpha}_1 \leq \bar{\alpha}_2$ in what follows.

Remark 5.1. While our analysis has been carried out on an infinite domain, in practice, the fully discrete numerical solution is necessarily calculated on a bounded domain. However, we can show that the theory is not very much affected by the bounded domain, as long as $\sqrt{\nu \Delta t} \ll L_\Omega$. Indeed, on a bounded domain, the solution is not exactly (17) but will involve matrices $\mathrm{e}^{\frac{-|x|}{\sqrt{\nu\Delta t}}\sqrt{A}}$ and $\mathrm{e}^{\frac{|x|}{\sqrt{\nu\Delta t}}\sqrt{A}}$ (as shown below in (A.2)), and the norm of the vector coefficient associated to the latter will become very small if $\sqrt{\nu \Delta t} \ll L_\Omega$. Thus, in our fully discrete numerical experiments, ν, Δt and L_Ω have been chosen so that they verify this condition.

Remark 5.2. As our analysis has been carried out in the semi-discrete in time case, we will take Δx small enough in the numerical experiments, to approach the discrete-time problem, *i.e.* we take $\Delta x \ll \sqrt{\nu \Delta t}$. However, when the previous condition is not satisfied, *e.g.* when $\Delta x = \Delta t$, we get similar numerical results.

[4] This means that in the OSWR algorithm we take $\alpha_i = \bar{\alpha}_i \sqrt{\frac{\nu}{\Delta t}}$, $i = 1, 2$.

[5] Similar results will be obtained if one takes the maximum of the L^∞-errors in the subdomains.

[6] One could also consider a scaling by $\|E^0_i(0)\|_\infty = \|\beta^0_i\|_\infty$ as in (31a), which will lead to similar results, if one takes random values for β^0_i, and then set $\bar{G}^0_i := (\bar{\alpha}_i \mathbf{I}_N - \sqrt{A})\beta^0_j$, $j = 3 - i$, $i = 1, 2$.

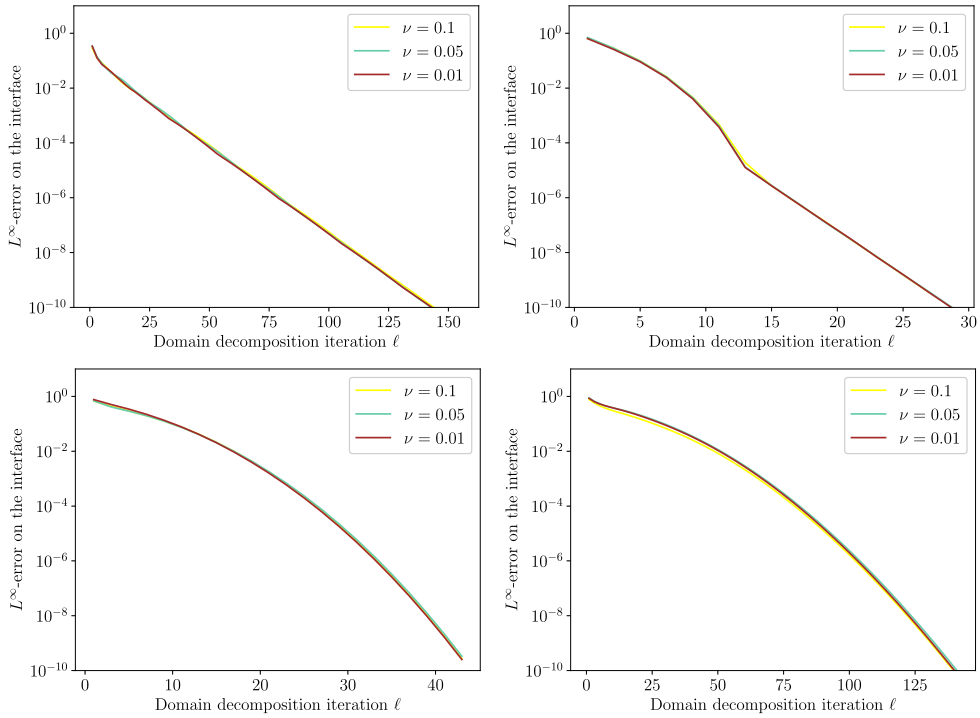

FIGURE 1. Illustration of convergence, which only depends on $\bar{\alpha}$, for a fixed N: L^∞-error, with $N = 100$ and different values of ν, for $\bar{\alpha} = 0.1$ (*top left*), $\bar{\alpha} = 0.5$ (*top right*), $\bar{\alpha} = 1$ (*bottom left*), $\bar{\alpha} = 3$ (*bottom right*).

Section 5.1 illustrates that, for a given $N \geq 1$, the convergence depends only on $\bar{\boldsymbol{\alpha}}$. Then, in Section 5.2, we verify that, at each OSWR iteration, the discrete-time convergence estimate is an accurate evaluation of the relative L^∞-error. Sections 5.3 and 5.4 illustrate the importance of choosing Robin parameters that are optimized for a targeted iteration count. In Section 5.5, asymptotic behaviors as a function of N are shown. Finally in Section 5.6, a comparison with $\bar{\alpha}_M$ and $\bar{\boldsymbol{\alpha}}_M$ (defined in (30)) is given.

In Sections 5.1–5.3 we consider one-sided Robin parameters $\bar{\alpha} := \bar{\alpha}_1 = \bar{\alpha}_2$. The case of two-sided parameters ($\bar{\alpha}_1$ and $\bar{\alpha}_2$ possibly different) will be treated in Section 5.4, and both cases will be considered in Sections 5.5 and 5.6.

5.1. Convergence depending only on $\bar{\alpha}$, for a given N

In this part we take $N = 100$. From Theorem 4.4 and Remark 4.5, we expect, for a fixed $\bar{\alpha}$, a convergence almost independent of ν when α is chosen as $\alpha = \bar{\alpha}\sqrt{\frac{\nu}{\Delta t}}$.

In Figure 1, we plot the evolution of the L^∞-error as a function of the number of iterations, for three values of ν (0.1, 0.05, 0.01). The four graphs correspond to four values of $\bar{\alpha}$ (0.1, 0.5, 1 and 3). We observe that the convergence is not influenced by the diffusion coefficient ν, as expected. As a consequence, in what follows, we only consider the case $\nu = 0.05$.

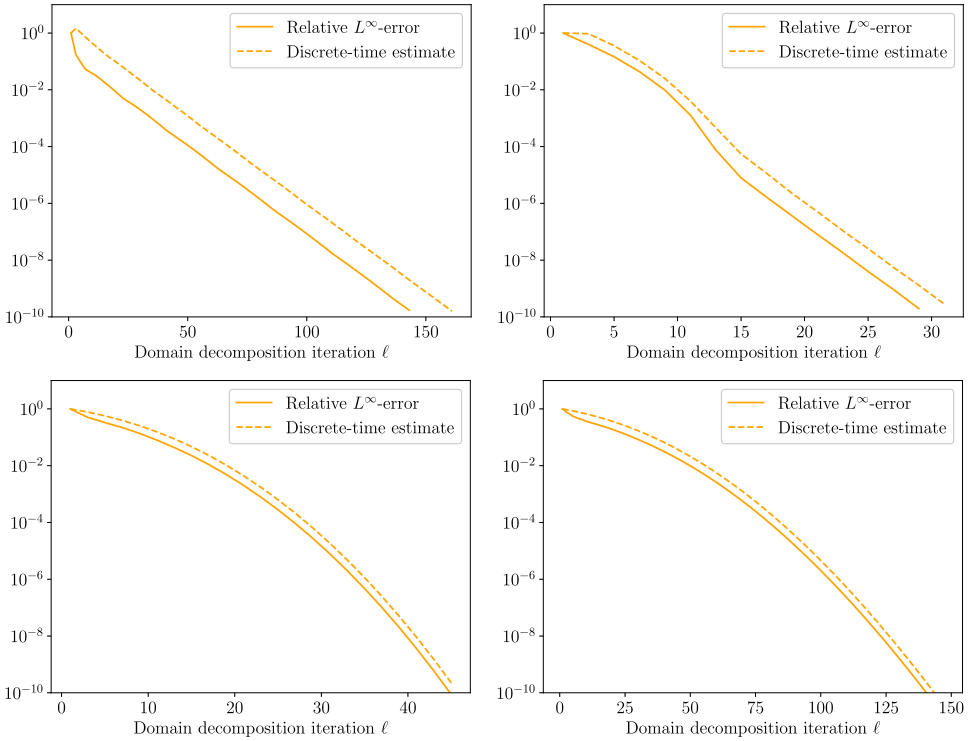

FIGURE 2. Comparison of relative L^∞-error (solid line) and discrete-time estimate (dashed line), for $N = 100$, with $\bar{\alpha} = 0.1$ (*top left*), $\bar{\alpha} = 0.5$ (*top right*), $\bar{\alpha} = 1$ (*bottom left*), $\bar{\alpha} = 3$ (*bottom right*).

5.2. Comparison between discrete-time estimate and relative L^∞-error

In this part, we show that the discrete-time convergence estimate $\|(M(\bar{\alpha}))^{q(\ell)}\|_\infty$ in (31) approaches well the relative L^∞-error, at each OSWR iteration ℓ, when the Robin initial guess has no particular structure, *e.g.* is a random vector, which implies that one cannot do better than going from equalities (24) to inequalities (25).

In Figure 2, we plot the relative L^∞-error (solid line) and the discrete-time estimate (dashed line), as functions of the number of iterations, for $N = 100$, and for different values of $\bar{\alpha}$ (0.1, 0.5, 1 and 3).

We observe that the discrete-time estimate is an upper bound of the relative L^∞-error, as expected from (31). Thus, we could not expect both curves to exactly overlay. However, the discrete-time estimates follow the actual relative L^∞-error curves, with very similar shapes, and are closer when $\bar{\alpha}$ is larger. A possible explanation for the differences is that the theoretical analysis of this paper is done on an infinite domain, while the numerical results are performed on the bounded domain $\left[-\frac{1}{2}, \frac{1}{2}\right]$. Another possible explanation is the loss of information when going from equalities (24) to inequalities (25).

Remark 5.3. Additional tests seem to show that changing the initial Robin data from random values to values with a particular structure, *e.g.* the Robin operator applied to $(u - u_0)$ as can be done in practice (where u is the solution of (1), and u_0 is the (time independent) initial condition) has a (limited) influence on the shapes of the relative L^∞-error curves, which are not as close to the discrete-time estimate as in the case of a random initial guess. In any case, the discrete-time estimates remain an upper bound of the actual error curves.

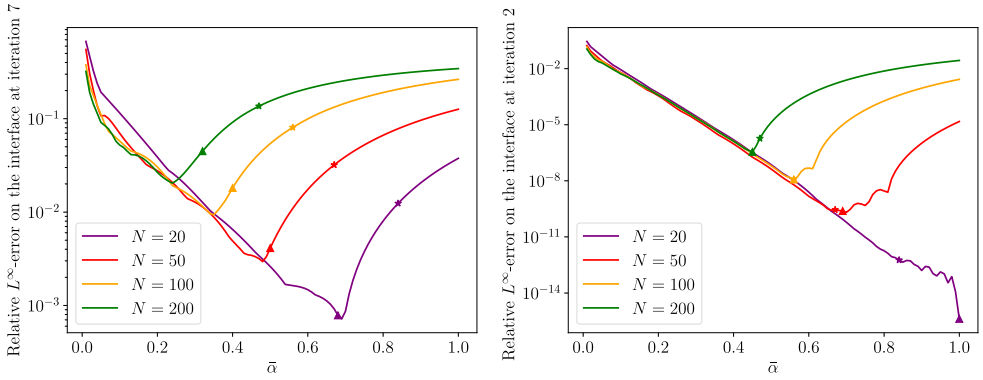

FIGURE 3. Relative L^∞-error on the interface as a function of $\bar{\alpha}$, at iteration 7 (*left*) and 21 (*right*). In each case, the triangles show $\bar{\alpha}_{D[7]}$ (*left*) and $\bar{\alpha}_{D[21]}$ (*right*), and the stars show $\bar{\alpha}_C$.

TABLE 1. Dimensionless *one-sided* Robin parameter optimized with continuous and discrete-time analysis, and numerical optimal parameter.

N	$\bar{\alpha}_C$	$\bar{\alpha}_{D[7]}$	$\bar{\alpha}_{\mathrm{opt}[7]}$	$\bar{\alpha}_{D[21]}$	$\bar{\alpha}_{\mathrm{opt}[21]}$
20	0.84	0.68	0.69	1.00	1.00
50	0.67	0.50	0.48	0.69	0.70
100	0.56	0.40	0.35	0.56	0.56
200	0.47	0.32	0.24	0.45	0.45

In this article, we intend to treat the most general case in which no information is known on the initial Robin data. Thus, in what follows, we focus on obtaining optimized dimensionless Robin parameters that minimize the discrete-time estimate, as done in Section 4.5, with random initial Robin values.

5.3. One-sided optimization

In this part, we consider *one-sided* Robin parameters ($\bar{\alpha}_1 = \bar{\alpha}_2$). We compute $\bar{\alpha}_{D[\ell]}$ using the method described in Remark 4.9.

5.3.1. Comparison of continuous and discrete-time parameters

In this section we compare the convergence obtained with the discrete-time optimized parameter $\bar{\alpha}_{D[\ell]}$ to those obtained with the continuous optimized parameter $\bar{\alpha}_C$ defined in (12) on the one hand, and with the actual numerical optimal one at iteration ℓ on the other hand. For this, we will consider two different iterations : $\ell = 7$ and $\ell = 21$.

On Figure 3 we plot the actual relative L^∞-error at iteration 7 (left) and at iteration 21 (right) *versus* the Robin parameter $\bar{\alpha}$. On these graphs, stars stand for continuous optimized Robin parameters $\bar{\alpha}_C$, and triangles are discrete-time optimized Robin parameters $\bar{\alpha}_{D[7]}$ (left) and $\bar{\alpha}_{D[21]}$ (right). Figure 3 allows to find the numerical optimal Robin parameter at iteration ℓ (for $\ell = 7$ and $\ell = 21$), denoted $\bar{\alpha}_{\mathrm{opt}[\ell]}$.

The values of $\bar{\alpha}_C$, $\bar{\alpha}_{\mathrm{opt}[7]}$, $\bar{\alpha}_{\mathrm{opt}[21]}$, $\bar{\alpha}_{D[7]}$, and $\bar{\alpha}_{D[21]}$ (rounded to the nearest hundredth), *versus* N, are reported in Table 1. Recall that $\bar{\alpha}_C$ is independent of the iterations, while $\bar{\alpha}_{D[7]}$ and $\bar{\alpha}_{D[21]}$ optimize iterations 7 and 21, respectively.

On Figure 3 (left) and in Table 1 we observe that, at iteration 7, for all values of N, the parameter $\bar{\alpha}_{D[7]}$ is close to the numerical optimal $\bar{\alpha}_{\mathrm{opt}[7]}$. The value of $\bar{\alpha}_{D[7]}$ deviates slightly from that of $\bar{\alpha}_{\mathrm{opt}[7]}$, when N increases; however the corresponding L^∞-error values remain close (within a factor of approximately 2, for $N = 200$). On

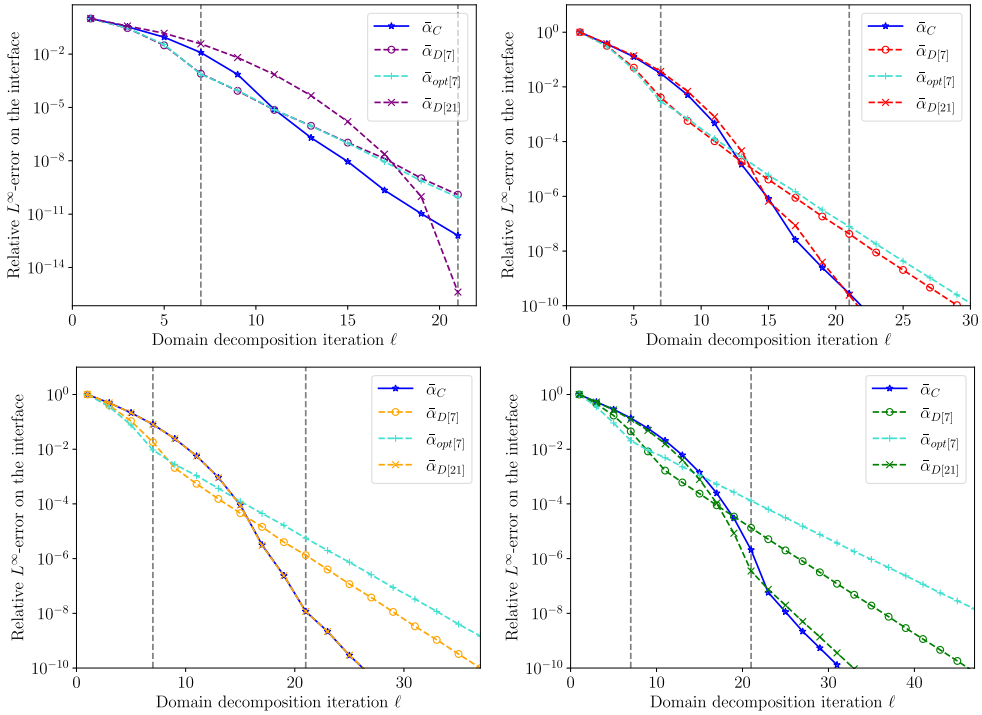

FIGURE 4. Relative L^∞-error computed with one-sided continuous, discrete-time (optimized at iteration $\ell = 7$ and 21) and numerical optimal (at iteration $\ell = 7$) Robin parameters, for $N = 20$ (*top left*), $N = 50$ (*top right*), $N = 100$ (*bottom left*), $N = 200$ (*bottom right*). Note the scale change for the top left figure (in that case convergence with $\bar{\alpha}_{D[21]} = 1$ is almost exact at the 21st iteration, as expected from Thm. 4.3). The curves with $\bar{\alpha}_{\text{opt}[21]}$ are not shown, since they are superimposed with those of $\bar{\alpha}_{D[21]}$.

Figure 3 (right) and Table 1, we see that at iteration 21 the parameter $\bar{\alpha}_{D[21]}$ is extremely close to the numerical optimal $\bar{\alpha}_{\text{opt}[21]}$. This is also the case for the parameter $\bar{\alpha}_C$, obtained by the continuous framework, except for $N = 200$. However, at iteration $\ell = 21$ for $N = 20$ and $N = 200$, and at iteration $\ell = 7$, for all N, the parameter $\bar{\alpha}_C$ is a worse approximation of $\bar{\alpha}_{\text{opt}[\ell]}$ than $\bar{\alpha}_{D[\ell]}$. This observation is crucial when one wants to perform a small number of iterations: in that case, the continuous optimization provides only a poor Robin coefficient and thus does not allow the OSWR algorithm to work efficiently.

On Figure 4, we plot the relative L^∞-error as a function of OSWR iterations (note the scale change for the top left figure), for different values of N, and with $\bar{\alpha}_C$, $\bar{\alpha}_{D[7]}$, $\bar{\alpha}_{\text{opt}[7]}$ and $\bar{\alpha}_{D[21]}$. Since the values of $\bar{\alpha}_{D[21]}$ and $\bar{\alpha}_{\text{opt}[21]}$ are extremely close for each N, the curves obtained with $\bar{\alpha}_{\text{opt}[21]}$ are not added on Figure 4.

We observe that at iteration 7 (resp. 21), the L^∞-error with $\bar{\alpha}_{D[7]}$ (resp. $\bar{\alpha}_{D[21]}$) is very close to the one obtained with $\bar{\alpha}_{\text{opt}[7]}$ (resp. $\bar{\alpha}_{\text{opt}[21]}$) and is smaller than the ones obtained with $\bar{\alpha}_C$. This confirms the relevance of choosing an optimized parameter that depends on the targeted iteration, as pointed out by the analysis. We also notice that, for $N \geq 50$, the curves obtained with $\bar{\alpha}_C$ and $\bar{\alpha}_{D[21]}$ are almost superimposed, since these Robin parameters are almost the same.

One of the main results of this article is that there is not a single Robin coefficient, independent of the iterations, that optimizes each iteration. Figures 3 and 4 illustrate this point: the numerical optimum varies according to ℓ; the parameter α_C, that minimizes the continuous convergence factor (which is independent of

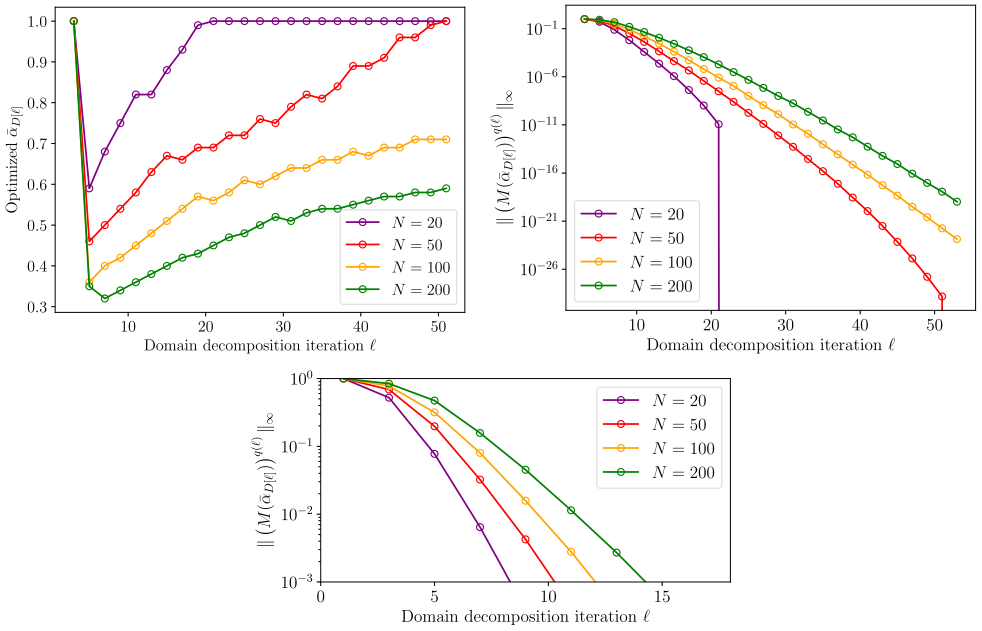

FIGURE 5. Discrete-time optimized Robin parameter $\bar{\alpha}_{D[\ell]}$ (*top left*) and associated discrete-time convergence estimate $\|(M(\bar{\alpha}_{D[\ell]}))^{q(\ell)}\|_\infty$ (*top right*), *versus* OSWR iterations, with a zoom on the first iterations (*bottom*).

the iteration), cannot optimize all iterations, whereas the method presented here allows to find a quite accurate approximation of the numerical optimum parameter, for each iteration ℓ.

5.3.2. Choice of an optimized pair $(\ell, \bar{\alpha})$ to reach a given accuracy

In this part, we give an abacus that allows to find an optimized pair $(\ell_{\mathrm{A}}, \bar{\alpha}_{D[\ell_{\mathrm{A}}]})$ to reach a given accuracy, *e.g.* the expected accuracy of the numerical scheme, or a fraction thereof.

Figure 5 shows, for different values of N, the values of $\bar{\alpha}_{D[\ell]}$ as a function of the targeted iteration count ℓ (top left figure), and the associated discrete-time estimate $\|(M(\bar{\alpha}_{D[\ell]}))^{q(\ell)}\|_\infty$ *versus* iteration ℓ (top right figure), with a zoom on the first iterations (bottom figure). With the cases $N = 20$ and $N = 50$, we see that for $\ell \geq N$ iterations, the discrete-time optimized Robin parameter is 1, as expected from Theorem 4.3. These numerical results also show that, after a few iterations, $\bar{\alpha}_{D[\ell]}$ is a globally increasing function of ℓ, that tends to 1, and a decreasing function of N.

Abacus 5.4 (How to choose ℓ and $\bar{\alpha}$ to reach a given accuracy)**.** Figure 5 allows to find an optimized pair $(\ell, \bar{\alpha}_{D[\ell]})$ to reach a given accuracy, *e.g.* the expected accuracy of the numerical scheme, or a fraction thereof. More precisely, the top right (or bottom) figure enables, for a given N, to find the minimum number ℓ of iterations one has to perform in order to reach a given error. Then, the top left figure gives the associated Robin parameter $\bar{\alpha}_{D[\ell]}$.

Let us now use the above abacus on an example. We choose f and the values of the boundary and initial conditions so that the continuous solution of (1) is given by $u(x,t) = (1 + t + t^2)(\sin(\pi x) + \cos(\pi x))$. The relative scheme error (between the fully discrete monodomain solution and the continuous solution) in L^∞-norm, denoted ε_{sch}, is given in Table 2 (first line), for different values of N. For each N, a pair $(\ell_{\mathrm{A}}, \bar{\alpha}_{D[\ell_{\mathrm{A}}]})$ is obtained by Abacus 5.4 to reach ε_{sch}, and is given in Table 2 (last two lines).

TABLE 2. Relative L^∞-error of the fully discrete numerical scheme on the interface, as a function of N, and associated optimized iteration ℓ_{A} and $\bar{\alpha}_{D[\ell_{\mathrm{A}}]}$ given by Abacus 5.4.

N	20	50	100	200
ε_{sch}	3.5×10^{-2}	1.4×10^{-2}	7.1×10^{-3}	3.6×10^{-3}
ℓ_{A}	7	9	11	13
$\bar{\alpha}_{D[\ell_{\mathrm{A}}]}$	0.68	0.54	0.45	0.38

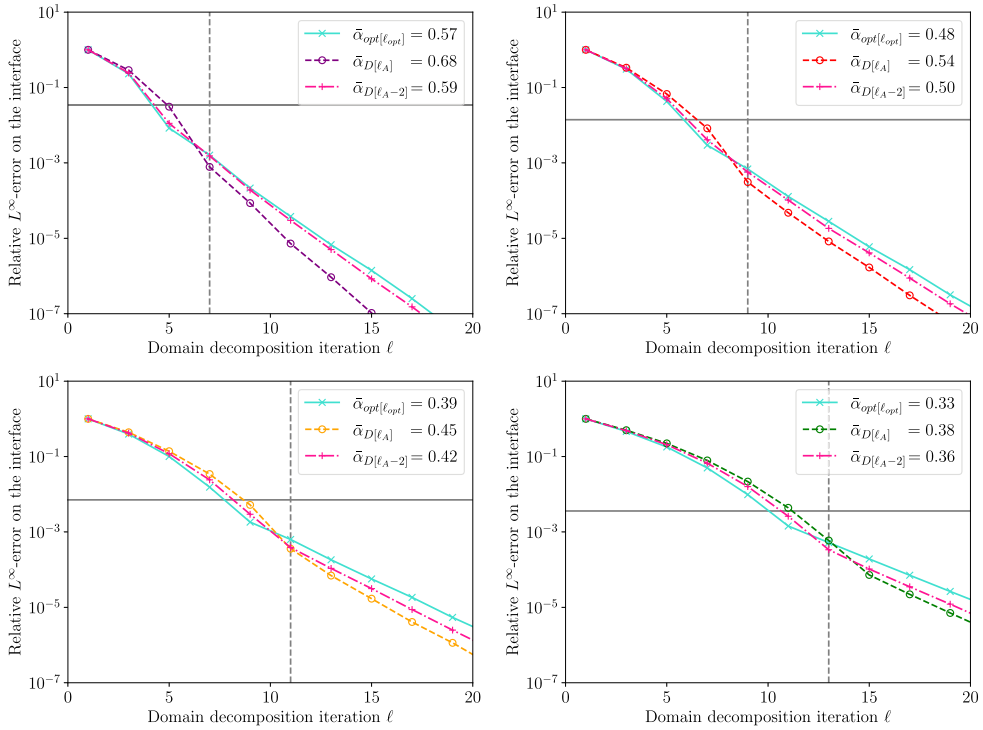

FIGURE 6. Relative L^∞-error computed with $\bar{\alpha}_{D[\ell_A]}$ provided by Abacus 5.4 for $N = 20$ (*top left*), $N = 50$ (*top right*), $N = 100$ (*bottom left*), $N = 200$ (*bottom right*). The error curves corresponding to $\bar{\alpha}_{D[\ell_{\mathrm{opt}}=\ell_{\mathrm{A}}-2]}$ and $\bar{\alpha}_{\mathrm{opt}[\ell_{\mathrm{opt}}]}$ are also shown, where ℓ_{opt} is the overall minimum (whatever the values of $\bar{\alpha}$) of iterations needed to reach the error scheme, represented by the horizontal line.

For example, for $N = 200$, if one wants to guarantee a relative L^∞-error smaller than $\varepsilon_{sch} = 3.6 \times 10^{-3}$, then from Figure 5 (top right or bottom) one only needs to perform thirteen iterations ($\ell_{\mathrm{A}} = 13$). Then Figure 5 (top left) gives the discrete-time optimized Robin parameter $\bar{\alpha}_{D[\ell_{\mathrm{A}}]} = \bar{\alpha}_{D[13]} = 0.38$.

Then, we choose $\bar{\alpha} = \bar{\alpha}_{D[\ell_{\mathrm{A}}]}$ in the actual simulation and plot on Figure 6 the corresponding relative L^∞-error (circle) curve as a function of OSWR iterations for the different values of N as well as a horizontal line corresponding to the scheme error (the other two curves of Fig. 6 are discussed below). Then, we check two important questions. The first is to know whether the actual error reached by choosing $\bar{\alpha} = \bar{\alpha}_{D[\ell_{\mathrm{A}}]}$ is indeed lower than ε_{sch} after ℓ_A iterations. This is the case, since we observe on Figure 6 that the circle located on the vertical dashed line is below the horizontal line. The second is to verify that the proposed value of ℓ_A iterations

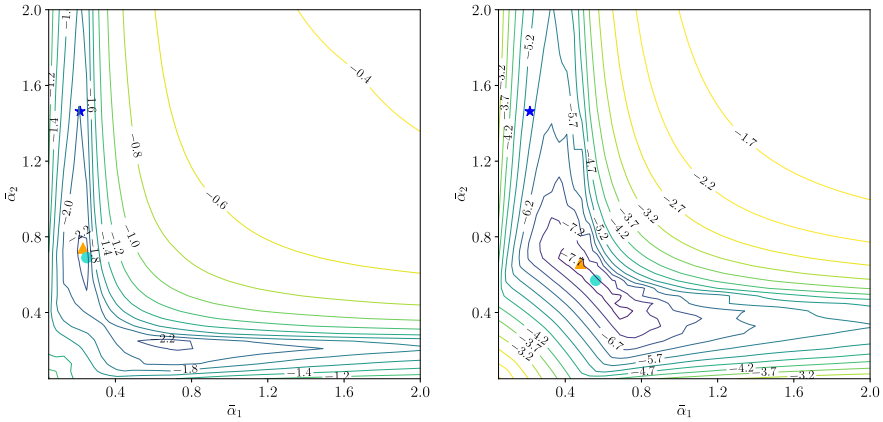

FIGURE 7. Level curves for the relative L^∞-error (in logarithmic scale) after 7 iterations (*left*), and 21 iterations (*right*), for various values of the parameters $\bar{\boldsymbol{\alpha}} = (\bar{\alpha}_1, \bar{\alpha}_2)$, for $N = 100$. The blue star shows $\bar{\boldsymbol{\alpha}}_C$, the orange triangle shows $\bar{\boldsymbol{\alpha}}_{D[7]}$ (*left*) and $\bar{\boldsymbol{\alpha}}_{D[21]}$ (*right*), and the cyan circle shows $\bar{\boldsymbol{\alpha}}_{\text{opt}[7]}$ (*left*) and $\bar{\boldsymbol{\alpha}}_{\text{opt}[21]}$ (*right*).

is equal, or at least close to the overall (whatever the values of $\bar{\alpha}$) minimum value ℓ_{opt} of iterations needed to reach ε_{sch}. This is also the case, since, in the examples that we treated, we found that $\ell_{\text{opt}} = \ell_A - 2$. This leads the practitioner to the following alternative: either one chooses the couple $(\ell_A, \bar{\alpha}_{D[\ell_A]})$ and this leads to a comfortable safety margin that ensures that the additional error due to domain decomposition is negligible with respect to the scheme error, or one chooses in a heuristic way the couple $(\ell_A - 2, \bar{\alpha}_{D[\ell_A - 2]})$ (pink curves on Fig. 6) and this leads to an error which is lower than the scheme error, close to the best possible error obtained in the optimal number of iterations ($(\ell_{\text{opt}}, \bar{\alpha}_{\text{opt}[\ell_{\text{opt}}]})$ cyan curves on Fig. 6).

5.4. Two-sided optimization

We now consider two-sided Robin parameters (*i.e.* $\bar{\alpha}_1$ and $\bar{\alpha}_2$ are possibly different), and more precisely the following ones:

- continuous $\bar{\boldsymbol{\alpha}}_C = (\bar{\alpha}_{1,C}, \bar{\alpha}_{2,C})$, defined in (12) (independent of the iterations);
- discrete-time $\bar{\boldsymbol{\alpha}}_{D[7]}$ that optimizes iteration 7, defined in (34) with $\ell = 7$;
- discrete-time $\bar{\boldsymbol{\alpha}}_{D[21]}$ that optimizes iteration 21, defined in (34) with $\ell = 21$.

We will compare the convergence obtained with these parameters to that obtained with the actual numerical optimal ones.

On Figure 7, we plot the level curves for the relative L^∞-error (in logarithmic scale) after 7 iterations (left), and 21 iterations (right), for various values of the two-sided Robin parameters $\bar{\boldsymbol{\alpha}} = (\bar{\alpha}_1, \bar{\alpha}_2)$, for $N = 100$. The blue star shows the continuous optimized parameter $\bar{\boldsymbol{\alpha}}_C$, the orange triangle shows the discrete-time optimized parameter $\bar{\boldsymbol{\alpha}}_{D[7]}$ (left figure) and $\bar{\boldsymbol{\alpha}}_{D[21]}$ (right figure). Figure 7 allows to find the numerical optimal Robin parameter at iteration ℓ (for $\ell = 7$ and $\ell = 21$), denoted $\bar{\boldsymbol{\alpha}}_{\text{opt}[\ell]}$, and represented by the cyan circle, for $N = 100$.

The values of $\bar{\boldsymbol{\alpha}}_C$, $\bar{\boldsymbol{\alpha}}_{\text{opt}[7]}$, $\bar{\boldsymbol{\alpha}}_{\text{opt}[21]}$, $\bar{\boldsymbol{\alpha}}_{D[7]}$, and $\bar{\boldsymbol{\alpha}}_{D[21]}$ (rounded to the nearest hundredth), *versus* N, are given in Table 3. For $N = 20,\ 50,\ 200$, the values of $\bar{\boldsymbol{\alpha}}_{\text{opt}[7]}$ and $\bar{\boldsymbol{\alpha}}_{\text{opt}[21]}$ are determined in a similar way to those of the case $N = 100$.

On Figure 7 and in Table 3, we observe that, at iteration 7 (resp. 21), the discrete-time optimized parameter $\bar{\boldsymbol{\alpha}}_{D[7]}$ (resp. $\bar{\boldsymbol{\alpha}}_{D[21]}$) is close to the numerical optimal $\bar{\boldsymbol{\alpha}}_{\text{opt}[7]}$ (resp. $\bar{\boldsymbol{\alpha}}_{\text{opt}[21]}$), and much closer to this optimal value than $\bar{\boldsymbol{\alpha}}_C$.

TABLE 3. Dimensionless *two-sided* Robin parameters optimized with continuous and discrete-time analysis, and numerical optimal parameters.

N	$\bar{\boldsymbol{\alpha}}_C$	$\bar{\boldsymbol{\alpha}}_{D[7]}$	$\bar{\boldsymbol{\alpha}}_{\mathrm{opt}[7]}$	$\bar{\boldsymbol{\alpha}}_{D[21]}$	$\bar{\boldsymbol{\alpha}}_{\mathrm{opt}[21]}$
20	$(0.56, 1.26)$	$(0.55, 0.86)$	$(0.69, 0.70)$	$(1.00, 1.00)$	$(1.00, 1.00)$
50	$(0.30, 1.49)$	$(0.33, 0.80)$	$(0.38, 0.74)$	$(0.68, 0.70)$	$(0.70, 0.71)$
100	$(0.21, 1.46)$	$(0.23, 0.74)$	$(0.25, 0.69)$	$(0.48, 0.66)$	$(0.56, 0.57)$
200	$(0.17, 1.33)$	$(0.16, 0.77)$	$(0.17, 0.77)$	$(0.30, 0.69)$	$(0.28, 0.64)$

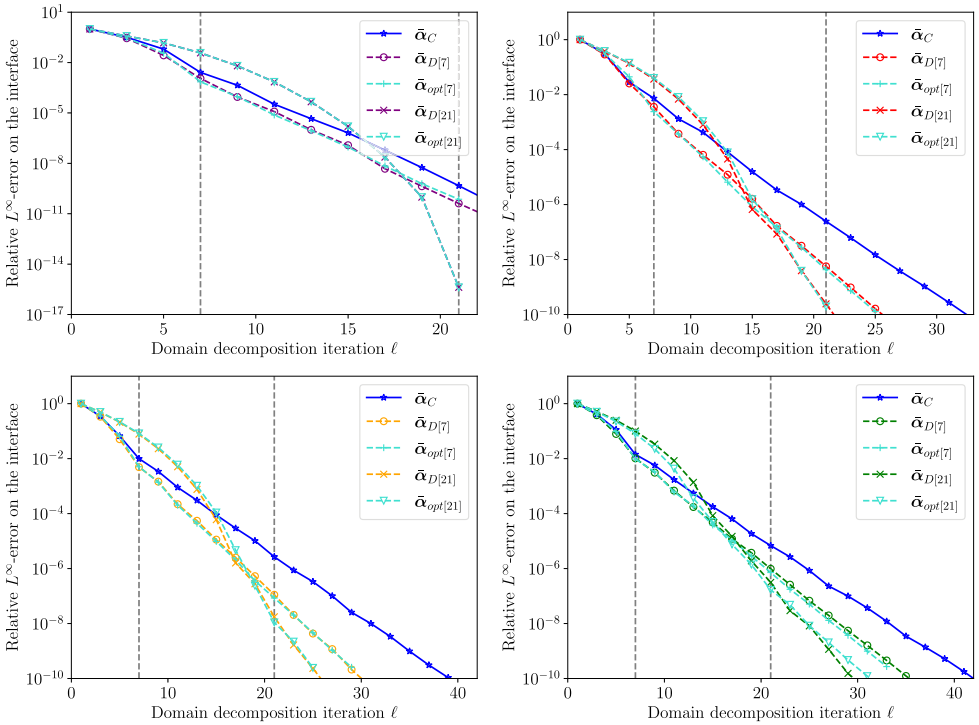

FIGURE 8. Relative L^∞-error computed with two-sided continuous, discrete-time (optimized at iteration $\ell = 7$ and 21) and numerical optimal (at iteration $\ell = 7$ and 21) Robin parameters, for $N = 20$ (*top left*), $N = 50$ (*top right*), $N = 100$ (*bottom left*), $N = 200$ (*bottom right*). Note the scale change for the top left figure, as explained in Figure 4. Note that, for $N = 20$, since $\bar{\boldsymbol{\alpha}}_{D[21]}$ and $\bar{\boldsymbol{\alpha}}_{\mathrm{opt}[21]}$ are equal, the associated curves are superimposed.

On Figure 8 we plot the relative L^∞-error as a function of OSWR iterations (note the scale change for the top left figure), obtained with these parameters.

As in the one-sided case, we observe that, at iteration 7 (resp. 21), the L^∞-error with $\bar{\boldsymbol{\alpha}}_{D[7]}$ (resp. $\bar{\boldsymbol{\alpha}}_{D[21]}$) is very close to the one obtained with $\bar{\boldsymbol{\alpha}}_{\mathrm{opt}[7]}$ (resp. $\bar{\boldsymbol{\alpha}}_{\mathrm{opt}[21]}$) and is smaller than the one obtained with $\bar{\boldsymbol{\alpha}}_C$. At iteration 7, the parameter $\bar{\boldsymbol{\alpha}}_C$ is a little less efficient than the discrete-time optimized parameter $\bar{\boldsymbol{\alpha}}_{D[7]}$. However, for a larger number of iterations (*e.g.* $\ell = 21$), $\bar{\boldsymbol{\alpha}}_C$ appears to be significantly less efficient than the discrete-time optimized parameter $\bar{\boldsymbol{\alpha}}_{D[21]}$. Again, we observe that the discrete-time optimized Robin coefficients proposed in this article allow to optimize efficiently the L^∞-error at a targeted iteration.

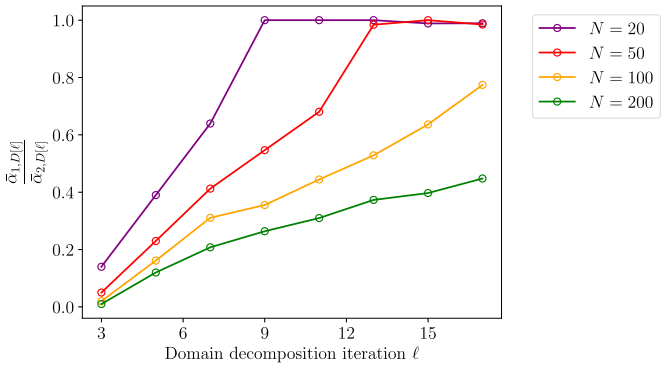

FIGURE 9. Ratio between discrete-time optimized two-sided Robin coefficients.

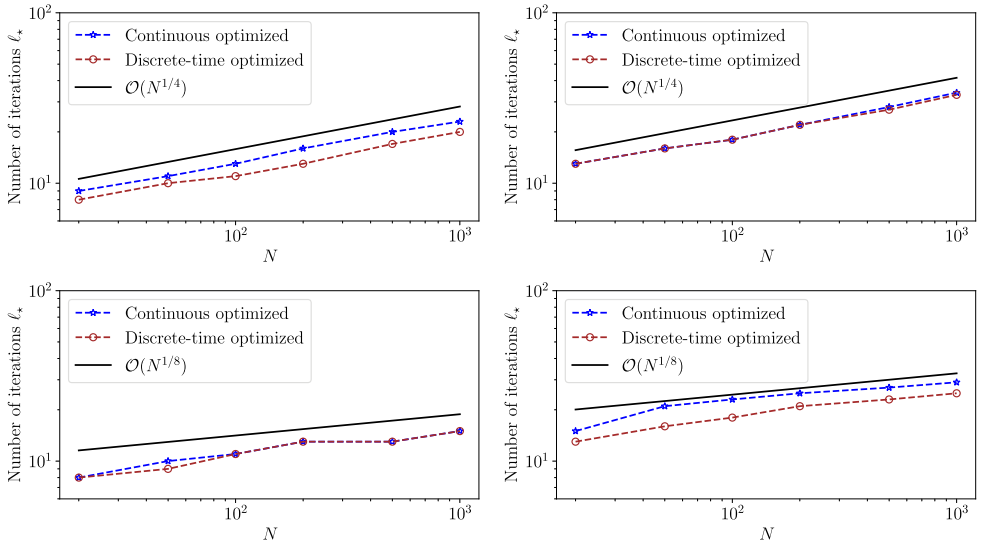

FIGURE 10. Asymptotic behavior: number of iterations $\ell_\star$ to obtain a relative L^∞-error smaller than 10^{-3} (*left figures*) and 10^{-6} (*right figures*), as a function of N, with $\Delta x = 5 \times 10^{-5}$, with continuous and discrete-time optimized parameters, in one-sided (*top*) and two-sided (*bottom*) cases.

Moreover, we notice that, the higher the number ℓ of domain decomposition iterations, the less $\bar{\alpha}_{1,D[\ell]}$ and $\bar{\alpha}_{2,D[\ell]}$ differ, as shown on Figure 9.

5.5. Asymptotic behavior as a function of N

In this part, we present the asymptotic performance as a function of N (or Δt), with continuous and discrete-time optimized parameters. Thus, we take $\Delta x = 5 \times 10^{-5}$ (to ensure $\Delta x \ll \sqrt{\nu \Delta t}$, see Rem. 5.2).

In Figure 10 we plot the number $\ell_\star$ of iterations that it takes to reduce the relative L^∞-error by a factor 10^{-3} (left figures) and 10^{-6} (right figures), as a function of N, on a log–log plot, in the one-sided case (top figures) and in the two-sided case (bottom figures). On top figures, the blue star curves are obtained with $\bar{\alpha}_C$, and the brown circle curves with $\bar{\alpha}_{D[\ell_A]}$, where $(\ell_A, \bar{\alpha}_{D[\ell_A]})$ is obtained by Abacus 5.4 to reach 10^{-3} (top left) and 10^{-6}

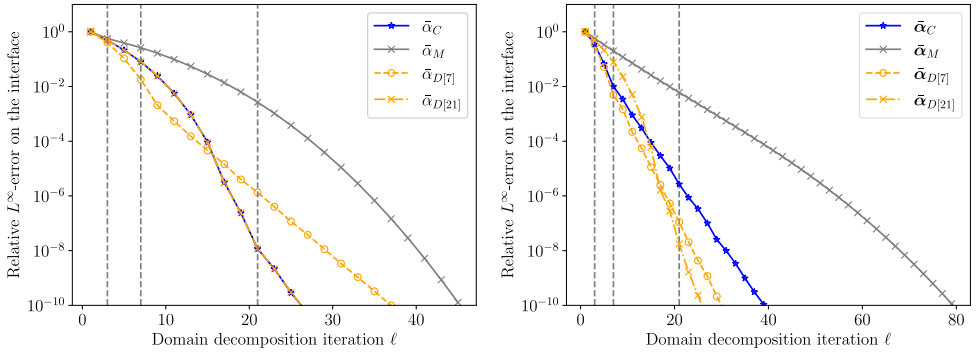

FIGURE 11. Comparison with parameters $\bar\alpha_M$ and $\bar{\boldsymbol\alpha}_M$: relative L^∞-errors computed with one-sided optimized parameters $\bar\alpha_C$, $\bar\alpha_M$, $\bar\alpha_{D[7]}$, $\bar\alpha_{D[21]}$ (*left*), and two-sided optimized parameters $\bar{\boldsymbol\alpha}_C$, $\bar{\boldsymbol\alpha}_M$, $\bar{\boldsymbol\alpha}_{D[7]}$, $\bar{\boldsymbol\alpha}_{D[21]}$ (*right*), for $\nu = 0.05$ and $N = 100$.

(top right); *e.g.* for $N = 200$, Abacus 5.4 gives $\ell_A = 23$ to reach 10^{-6}, then, choosing $\bar\alpha = \bar\alpha_{D[23]} (= \bar\alpha_{D[22]}$ from Definition (33)) in the actual simulation, one needs $\ell_\star = 22$ iterations to actually reach the relative accuracy 10^{-6}. We proceed similarly in the two-sided case (bottom figures).

Using that $\Delta t = \frac{T}{N}$, the numerical results show the following asymptotic behaviors:

- $\ell_\star = \mathcal{O}(N^{\frac{1}{4}}) = \mathcal{O}(\Delta t^{-\frac{1}{4}})$ in the one-sided case, both for discrete-time and continuous optimized parameters (as predicted in [15] for the latter);
- $\ell_\star = \mathcal{O}(N^{\frac{1}{8}}) = \mathcal{O}(\Delta t^{-\frac{1}{8}})$ in the two-sided case, both for discrete-time and continuous optimized parameters.

The curves on Figure 10 show that discrete-time and continuous optimized parameters give similar asymptotic behaviors *versus* N (or Δt), depending only a little on N (or Δt) for one-sided (increasing approximately by a factor 2 when N is multiplied by a factor 16), and almost independent of N (or Δt) for two-sided parameters (increasing approximately by a factor 2 when N is multiplied by a factor 256).

5.6. Comparison with $\bar{\boldsymbol\alpha}_M$

In this test, we take $N = 100$. Figure 11 shows the relative L^∞-errors as a function of OSWR iterations, obtained with $\bar\alpha_M$ and $\bar{\boldsymbol\alpha}_M$ defined in (30), compared to those obtained with continuous and discrete-time optimized parameters. Using Remark 4.10, we find $\bar\alpha_M = 1$ and $\bar{\boldsymbol\alpha}_M = (0.02, 1)$. We observe that, except for the very first iterations, the convergence with $\bar\alpha_M$ (left) or $\bar{\boldsymbol\alpha}_M$ (right) is much slower than with the other parameters.

6. CONCLUSION

We have observed that the numerical optimal Robin parameter varies according to the performed number of OSWR iterations; therefore the continuous optimized parameter (which is independent of this number) cannot optimize all iterations, whereas the method presented here allows to find a quite accurate approximation of the numerical optimal parameter, for each OSWR iteration count, and allows to find an optimized pair $(\ell, \bar\alpha_{D[\ell]})$ to reach a given accuracy.

As a perspective, we have noted in Remark 5.3 that changing the initial Robin data influences the shapes of the convergence curves, in particular those of Figures 2 and 3. Therefore, additional analysis is required to further improve the choice of the Robin parameter. Note also that, as shown in [18,19], taking into account the effect of spatial discretization in the methodology to choose optimized Robin parameters is not trivial. Finally,

the extension to other time schemes is currently under investigation. For these two issues, additional work is needed.

Appendix A. Proof of Theorem 4.1

Proof. Let us first consider the problem in Ω_1 in (14): find U such that

$$\begin{aligned} &LU = 0 && \text{in } \Omega_1, \\ &\lim_{x\to-\infty} U(x) && \text{is bounded.} \end{aligned} \tag{A.1}$$

From Proposition 3.10 and equation (7), the matrix $C := \frac{1}{\sqrt{\nu\Delta t}}\sqrt{A}$ is lower triangular, invertible, with all its diagonal coefficients equal to $\frac{1}{\sqrt{\nu\Delta t}} > 0$.

Setting $Z := \begin{pmatrix} U' \\ U \end{pmatrix}$, $\chi := U'(x=0)$, $\Psi := U(x=0)$, and $M := \begin{pmatrix} 0 & C^2 \\ I & 0 \end{pmatrix}$, then problem (A.1) can be written into the equivalent first order differential system

$$\begin{aligned} &Z' = MZ && \text{in } (-\infty, 0), \\ &Z(x=0) = (\chi, \Psi)^T, \\ &Z && \text{is bounded in } (-\infty, 0). \end{aligned}$$

The solution of the above problem is given by

$$Z(x) = \mathrm{e}^{xM}\begin{pmatrix} \chi \\ \Psi \end{pmatrix}, \qquad \forall x \in (-\infty, 0).$$

Using that $M^2 = \begin{pmatrix} C^2 & 0 \\ 0 & C^2 \end{pmatrix}$, we get by induction $M^{2k} = \begin{pmatrix} C^{2k} & 0 \\ 0 & C^{2k} \end{pmatrix}$ and $M^{2k+1} = \begin{pmatrix} 0 & C^{2k+2} \\ C^{2k} & 0 \end{pmatrix}$, $\forall k \in \mathbb{N}$, and thus

$$\begin{aligned} \mathrm{e}^{xM} &= \sum_{k=0}^{+\infty} \frac{x^{2k}}{2k!} M^{2k} + \sum_{k=0}^{+\infty} \frac{x^{2k+1}}{(2k+1)!} M^{2k+1} \\ &= \sum_{k=0}^{+\infty} \frac{x^{2k}}{2k!} \begin{pmatrix} C^{2k} & 0 \\ 0 & C^{2k} \end{pmatrix} + \sum_{k=0}^{+\infty} \frac{x^{2k+1}}{(2k+1)!} \begin{pmatrix} 0 & C^{2k+1}C \\ C^{2k+1}C^{-1} & 0 \end{pmatrix} \\ &= \begin{pmatrix} \mathrm{ch}(xC) & 0 \\ 0 & \mathrm{ch}(xC) \end{pmatrix} + \begin{pmatrix} 0 & \mathrm{sh}(xC)C \\ \mathrm{sh}(xC)\,C^{-1} & 0 \end{pmatrix} \\ &= \begin{pmatrix} \mathrm{ch}(xC) & \mathrm{sh}(xC)C \\ \mathrm{sh}(xC)C^{-1} & \mathrm{ch}(xC) \end{pmatrix}. \end{aligned}$$

Then we have, $\forall x \in (-\infty, 0)$,

$$\begin{pmatrix} U'(x) \\ U(x) \end{pmatrix} = \begin{pmatrix} \mathrm{ch}(xC) & \mathrm{sh}(xC)C \\ \mathrm{sh}(xC)C^{-1} & \mathrm{ch}(xC) \end{pmatrix} \begin{pmatrix} \chi \\ \Psi \end{pmatrix},$$

from which we obtain, $\forall x \in (-\infty, 0)$,

$$U(x) = \mathrm{sh}(xC)C^{-1}\chi + \mathrm{ch}(xC)\Psi.$$

The solutions of the system can therefore be written as follows

$$U(x) = \mathrm{e}^{xC}\beta^+ + \mathrm{e}^{-xC}\beta^-, \tag{A.2}$$

where $\beta^+ \in \mathbb{R}^N$ and $\beta^- \in \mathbb{R}^N$ will be determined using the boundary conditions.

More precisely, let us show that the condition U is bounded in $(-\infty, 0)$ implies that $\beta^- = 0_N$. We set

$$\mathcal{E}(x) \coloneqq \exp(-xC)\beta^-. \tag{A.3}$$

Since C is lower triangular, so are the sums and multiples of C. Coming back to the definition of the exponential of a matrix (with power series), we deduce that $\exp(-xC)$ is a lower triangular matrix whose diagonal is only composed of the exponential of $-\frac{x}{\sqrt{\nu\Delta t}}$. Thus, the first line of (A.3) gives $(\mathcal{E}(x))_1 = \mathrm{e}^{\frac{-x}{\sqrt{\nu\Delta t}}}(\beta^-)_1$, with $\frac{1}{\sqrt{\nu\Delta t}} > 0$. Since U (and thus $\mathcal{E}$) is bounded as x tends to $-\infty$, we deduce that $(\beta^-)_1 = 0$. Then, the second line of (A.3) gives $(\beta^-)_2 = 0$, and by induction we obtain $\beta^- = 0_N$. Thus, the solutions of (A.1) are of the form $U(x) = \mathrm{e}^{xC}\beta^+$, with $\beta^+ \in \mathbb{R}^N$. The problem in Ω_2 is treated similarly to that in Ω_1, by using a change of variables, which ends the proof of Theorem 4.1. □

References

[1] E. Ahmed, C. Japhet and M. Kern, Space-time domain decomposition for two-phase flow between different rock types. *Comput. Methods Appl. Mech. Eng.* **371** (2020) 113294.

[2] S. Ali Hassan, C. Japhet and M. Vohralík, A posteriori stopping criteria for space-time domain decomposition for the heat equation in mixed formulations. *Electron. Trans. Numer. Anal.* **49** (2018) 151–181.

[3] D. Bennequin, M.J. Gander, L. Gouarin and L. Halpern, Optimized Schwarz waveform relaxation for advection reaction diffusion equations in two dimensions. *Numer. Math.* **134** (2016) 513–567.

[4] P.-M. Berthe, C. Japhet and P. Omnes, Space-time domain decomposition with finite volumes for porous media applications, in Domain Decomposition Methods in Science and Engineering XXI, edited by J. Erhel, M.J. Gander, L. Halpern, G. Pichot, T. Sassi and O. Widlund. Springer International Publishing, Cham (2014) 567–575.

[5] E. Blayo, L. Halpern and C. Japhet, Optimized Schwarz waveform relaxation algorithms with nonconforming time discretization for coupling convection-diffusion problems with discontinuous coefficients, in Domain Decomposition Methods in Science and Engineering XVI, edited by O.B. Widlund and D.E. Keyes. Springer Berlin Heidelberg, Berlin, Heidelberg (2007) 267–274.

[6] E. Blayo, A. Rousseau and M. Tayachi, Boundary conditions and Schwarz waveform relaxation method for linear viscous Shallow Water equations in hydrodynamics. *SMAI J. Comput. Math.* **3** (2017) 117–137.

[7] D.Q. Bui, C. Japhet, Y. Maday and P. Omnes, Coupling parareal with optimized Schwarz waveform relaxation for parabolic problems. *SIAM J. Numer. Anal.* **60** (2022) 913–939.

[8] O. Ciobanu, L. Halpern, X. Juvigny and J. Ryan, Overlapping domain decomposition applied to the Navier–Stokes equations, in Domain Decomposition Methods in Science and Engineering XXII, edited by T. Dickopf, M.J. Gander, L. Halpern, R. Krause and L.F. Pavarino. Springer International Publishing, Cham (2016) 461–470.

[9] S. Clement, F. Lemarié and E. Blayo, Discrete analysis of Schwarz waveform relaxation for a diffusion reaction problem with discontinuous coefficients. *SMAI J. Comput. Math.* **8** (2022) 99–124.

[10] S. Descombes, V. Dolean and M.J. Gander, Schwarz waveform relaxation methods for systems of semi-linear reaction-diffusion equations, in Domain Decomposition Methods in Science and Engineering XIX, edited by Y. Huang, R. Kornhuber, O. Widlund and J. Xu. Springer Berlin Heidelberg, Berlin, Heidelberg (2011) 423–430.

[11] J.W. Eaton, D. Bateman, S. Hauberg and R. Wehbring, GNU Octave version 7.1.0 manual: a high-level interactive language for numerical computations (2022).

[12] M.J. Gander, Overlapping Schwarz waveform relaxation for parabolic problems, in Tenth International Conference on Domain Decomposition Methods. Contemporary Mathematics, edited by J. Mandel, C. Farhat and X.-C. Cai. Vol. 218. AMS, Boulder, CO (1998).

[13] M.J. Gander, Optimized Schwarz methods. SIAM *J. Numer. Anal.* **44** (2006) 699–731.

[14] M.J. Gander and L. Halpern, Méthodes de relaxation d'ondes (SWR) pour l'équation de la chaleur en dimension 1. (Optimized Schwarz waveform relaxation (SWR) for the one-dimensional heat equation). *C. R. Math. Acad. Sci. Paris* **336** (2003) 519–524.

[15] M.J. Gander and L. Halpern, Optimized Schwarz waveform relaxation methods for advection reaction diffusion problems. *SIAM J. Numer. Anal.* **45** (2007) 666–697.

[16] M.J. Gander and V. Martin, A detailed Fourier mode analysis of Schwarz waveform relaxation methods, in Contributed lecture at the 27th International Domain Decomposition Conference. DD27, Prague, Czech Republic (2022).

[17] M.J. Gander and A.M. Stuart, Space-time continuous analysis of waveform relaxation for the heat equation. *SIAM J. Sci. Comput.* **19** (1998) 2014–2031.

[18] M.J. Gander, L. Halpern, F. Hubert and S. Krell, Discrete optimization of robin transmission conditions for anisotropic diffusion with discrete duality finite volume methods. *Vietnam J. Math.* **49** (2021) 1349–1378.

[19] M.J. Gander, L. Halpern, F. Hubert and S. Krell, Optimized Schwarz methods with general ventcell transmission conditions for fully anisotropic diffusion with discrete duality finite volume discretizations. *Moroccan J. Pure Appl. Anal.* **7** (2021) 182–213.

[20] M.J. Gander, L. Halpern and F. Nataf, Optimal Schwarz waveform relaxation for the one dimensional wave equation. *SIAM J. Numer. Anal.* **41** (2003) 1643–1681.

[21] M.J. Gander, Y. Jiang and B. Song, A superlinear convergence estimate for the parareal Schwarz waveform relaxation algorithm. *SIAM J. Sci. Comput.* **41** (2019) A1148–A1169.
[22] E. Giladi and H. Keller, Space-time domain decomposition for parabolic problems. *Numer. Math.* **93** (2002) 279–313.
[23] G.H. Golub and C.F. Van Loan, Matrix Computations. Johns Hopkins University Press (1996).
[24] R. Guetat, *Méthode de parallélisation en temps: application aux méthodes de décomposition de domaine*. Ph.D. thesis, UPMC Université Paris 6 et Ecole polytechnique de Tunisie (2011).
[25] F. Haeberlein, *Méthodes de décomposition de domaine espace temps pour le transport réactif: Application au stockage géologique de CO_2*. Ph.D. thesis, Université Paris 13 (2011).
[26] L. Halpern, C. Japhet and J. Szeftel, Optimized Schwarz waveform relaxation and discontinuous Galerkin time stepping for heterogeneous problems. *SIAM J. Numer. Anal.* **50** (2012) 2588–2611.
[27] R.D. Haynes and K. Mohammad, Fully discrete Schwarz waveform relaxation on two bounded overlapping subdomains, in Domain Decomposition Methods in Science and Engineering XXV, R. Haynes, S. MacLachlan, X.-C. Cai, L. Halpern, H.H. Kim, A. Klawonn and O. Widlund. Springer International Publishing, Cham (2020) 159–166.
[28] T.-T.-P. Hoang, J. Jaffré, C. Japhet, M. Kern and J.E. Roberts, Space-time domain decomposition methods for diffusion problems in mixed formulations. *SIAM J. Numer. Anal.* **51** (2013) 3532–3559.
[29] T.-T.-P. Hoang, C. Japhet, M. Kern and J.E. Roberts, Space-time domain decomposition for reduced fracture models in mixed formulation. *SIAM J. Numer. Anal.* **54** (2016) 288–316.
[30] C. Japhet and F. Nataf, The best interface conditions for domain decomposition methods: absorbing boundary conditions, in Absorbing Boundaries and Layers, Domain Decomposition Methods. Nova Sci. Publ., Huntington, NY (2001) 348–373.
[31] C. Japhet, F. Nataf and F. Rogier, The optimized order 2 method: application to convection-diffusion problems. *Future Gener. Comput. Syst.* **18** (2001) 17–30.
[32] P.-L. Lions, On the Schwarz alternating method. III: a variant for nonoverlapping subdomains, in Third International Symposium on Domain Decomposition Methods for Partial Differential Equations, held in Houston, Texas, March 20–22, 1989, edited by T.F. Chan, R. Glowinski, J. Périaux and O. Widlund. SIAM, Philadelphia, PA (1990) 202–223.
[33] J.-L. Lions and E. Magenes, Non-Homogeneous Boundary Value Problems and Applications. Translated from the French by P. Kenneth, Die Grundlehren der mathematischen Wissenschaften, Band 181. Vol. I. Springer-Verlag, New York (1972).
[34] J.-L. Lions and E. Magenes, Non-Homogeneous Boundary Value Problems and Applications. Translated from the French by P. Kenneth, Die Grundlehren der mathematischen Wissenschaften, Band 182. Vol. II. Springer-Verlag, New York (1972).
[35] V. Martin, An optimized Schwarz waveform relaxation method for the unsteady convection diffusion equation in two dimensions. *Appl. Numer. Math.* **52** (2005) 401–428.
[36] V. Martin, Schwarz waveform relaxation algorithms for the linear viscous equatorial shallow water equations. *SIAM J. Sci. Comput.* **31** (2009) 3595–3625.
[37] D. Serre, Les matrices – Théorie et pratique. Dunod (2001).
[38] S. Thery, On the links between observed and theoretical convergence rates for Schwarz waveform relaxation algorithm for the time-dependent problems, in 26th International Domain Decomposition Conference, Dec 2020. Hong Kong, China (2020).
[39] S. Thery, C. Pelletier, F. Lemarié and E. Blayo, Analysis of Schwarz waveform relaxation for the coupled Ekman boundary layer problem with continuously variable coefficients. *Numer. Algorithms* **89** (2022) 1145–1181.
[40] C.W. Ueberhuber, Numerical Computation 2. Springer (1995).
[41] S.-L. Wu, Schwarz waveform relaxation algorithm for heat equations with distributed delay. *Therm. Sci.* **20** (2016) 659–667.

Please help to maintain this journal in open access!

This journal is currently published in open access under the Subscribe to Open model (S2O). We are thankful to our subscribers and supporters for making it possible to publish this journal in open access in the current year, free of charge for authors and readers.

Check with your library that it subscribes to the journal, or consider making a personal donation to the S2O programme by contacting subscribers@edpsciences.org.

More information, including a list of supporters and financial transparency reports, is available at https://edpsciences.org/en/subscribe-to-open-s2o.